Chapter 5

Hadron calorimeter

The CMS detector is designed to study a wide range of high-energy processes involving diverse signatures of final states. The hadron calorimeters are particularly important for the measurement of hadron jets and neutrinos or exotic particles resulting in apparent missing transverse energy [1].

Figure 5.1 shows the longitudinal view of the CMS detector. The dashed lines are at fixed η values. The hadron calorimeter barrel and endcaps sit behind the tracker and the electromagnetic calorimeter as seen from the interaction point. The hadron calorimeter barrel is radially restricted between the outer extent of the electromagnetic calorimeter (R = 1.77 m) and the inner extent of the magnet coil (R = 2.95 m). This constrains the total amount of material which can be put in to absorb the hadronic shower. Therefore, an outer hadron calorimeter or *tail catcher* is placed outside the solenoid complementing the barrel calorimeter. Beyond $|\eta| = 3$, the forward hadron calorimeters placed at 11.2 m from the interaction point extend the pseudorapidity coverage down to $|\eta| = 5.2$ using a Cherenkov-based, radiation-hard technology. The following sections describe these subdetectors in detail.

5.1 Barrel design (HB)

The HB is a sampling calorimeter covering the pseudorapidity range $|\eta| < 1.3$. The HB is divided into two half-barrel sections (figure 5.2), each half-section being inserted from either end of the barrel cryostat of the superconducting solenoid and subsequently hung from rails in the median plane. Since the HB is very rigid compared to the cryostat, great care has been taken to ensure that the barrel load is distributed evenly along the rails [108].

Absorber geometry

The HB consists of 36 identical azimuthal wedges which form the two half-barrels (HB+ and HB–). The wedges are constructed out of flat brass absorber plates (table 5.1) aligned parallel to the beam axis. The numbering scheme of the wedges is shown in figure 5.3. Each wedge is segmented into four azimuthal angle (ϕ) sectors. The plates are bolted together in a staggered geometry resulting in a configuration that contains no projective dead material for the full radial extent of a wedge (figure 5.4). The innermost and outermost plates are made of stainless steel for structural strength. The plastic scintillator is divided into 16 η sectors, resulting in a segmentation

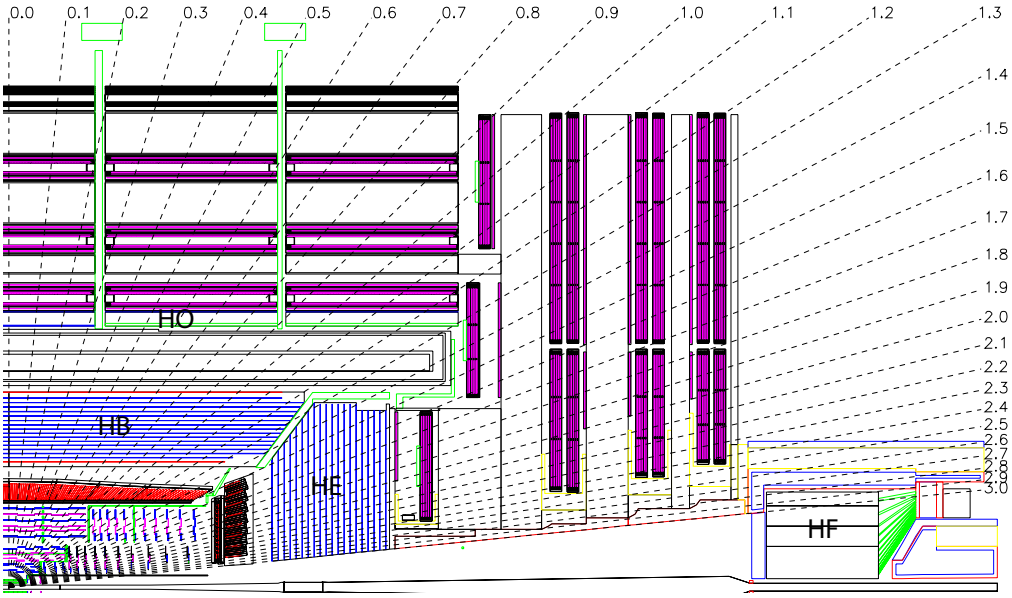

Figure 5.1: Longitudinal view of the CMS detector showing the locations of the hadron barrel (HB), endcap (HE), outer (HO) and forward (HF) calorimeters.

Table 5.1: Physical properties of the HB brass absorber, known as C26000/cartridge brass.

chemical composition	70% Cu, 30% Zn
density	8.53 g/cm^3
radiation length	1.49 cm
interaction length	16.42 cm

$(\Delta\eta, \Delta\phi) = (0.087, 0.087)$. The wedges are themselves bolted together, in such a fashion as to minimize the crack between the wedges to less than 2 mm.

The absorber (table 5.2) consists of a 40-mm-thick front steel plate, followed by eight 50.5-mm-thick brass plates, six 56.5-mm-thick brass plates, and a 75-mm-thick steel back plate. The total absorber thickness at 90° is 5.82 interaction lengths (λ_I). The HB effective thickness increases with polar angle (θ) as $1/\sin\theta$, resulting in 10.6 λ_I at $|\eta| = 1.3$. The electromagnetic crystal calorimeter [69] in front of HB adds about 1.1 λ_I of material.

Scintillator

The active medium uses the well known tile and wavelength shifting fibre concept to bring out the light. The CMS hadron calorimeter consists of about 70 000 tiles. In order to limit the number of individual elements to be handled, the tiles of a given ϕ layer are grouped into a single mechanical scintillator tray unit. Figure 5.5 shows a typical tray. The tray geometry has allowed for construction and testing of the scintillators remote from the experimental installation area. Furthermore,

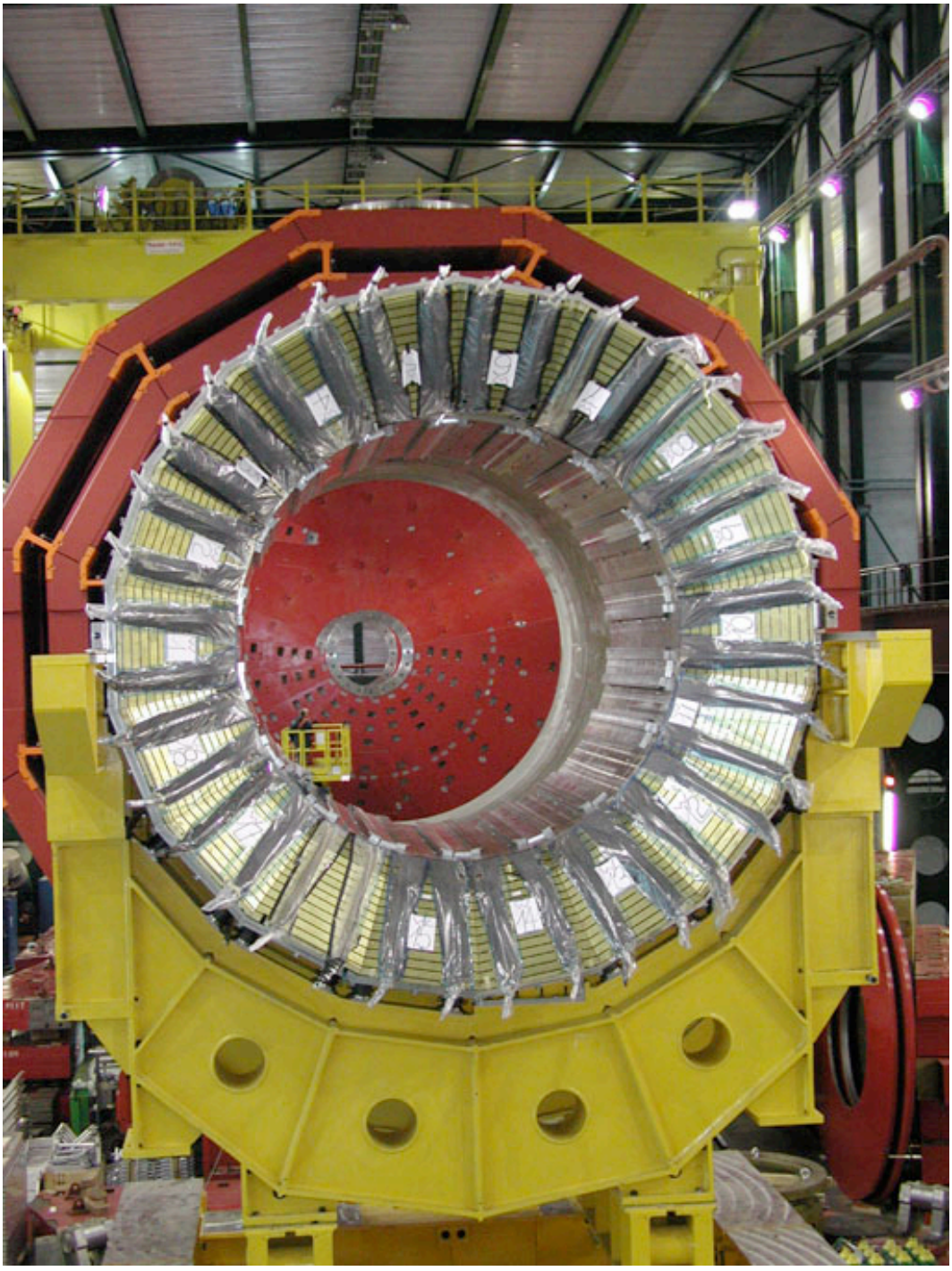

Figure 5.2: Assembled HCAL half-barrel in SX5, the above ground assembly hall.

individual scintillator trays may be replaced without disassembly of the absorber in the event of catastrophic damage. Each HB wedge has four ϕ divisions (ϕ-index = 1–4). Trays with segmentation of ϕ-index 2 and 3 go into the center of a wedge while trays with segmentation of ϕ-index 1 and 4 go into the edge slots in a wedge (figure 5.4). Each layer has 108 trays. Figure 5.6 shows a cross section of the tray.

2008 JINST 3 S08004

Table 5.2: Absorber thickness in the HB wedges.

layer	*material*	*thickness*
front plate	steel	40 mm
1-8	brass	50.5 mm
9-14	brass	56.5 mm
back plate	steel	75 mm

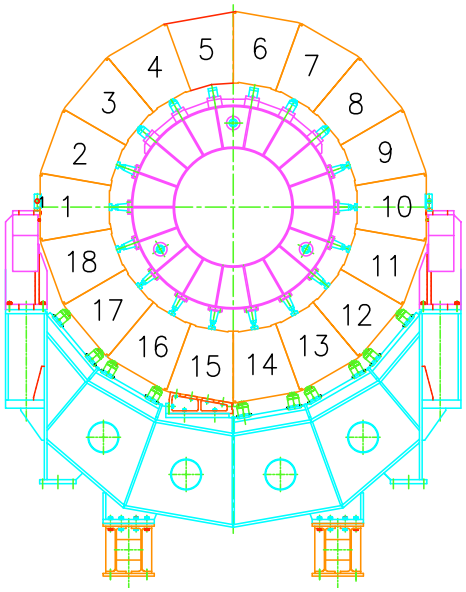

Figure 5.3: Numbering scheme for the HB wedges. Wedge 1 is on the inside ($+x$ direction) of the LHC ring.

The HB baseline active material is 3.7-mm-thick Kuraray SCSN81 plastic scintillator, chosen for its long-term stability and moderate radiation hardness. The first layer of scintillator (layer 0) is located in front of the steel support plate. It was originally foreseen to have a separate read-out [108] and is made of 9-mm-thick Bicron BC408. The scintillators are summarized in table 5.3. The purpose of layer zero is to sample hadronic showers developing in the inert material between the EB and HB. The larger thickness of layer 16 serves to correct for late developing showers leaking out the back of HB.

A tray is made of individual scintillators with edges painted white and wrapped in Tyvek 1073D which are attached to a 0.5-mm-thick plastic substrate with plastic rivets. Light from each tile is collected with a 0.94-mm-diameter green double-cladded wavelength-shifting fibre (Kuraray Y-11) placed in a machined groove in the scintillator. For calibration purposes, each tray has 1-mm-diameter stainless steel tubes, called *source tubes*, that carry Cs^{137} (or optionally Co^{60}) radioactive sources through the center of each tile. An additional quartz fibre is used to inject ultraviolet (337 nm) laser light into the layer 9 tiles. The top of the tray is covered with 2-mm-thick white polystyrene. The cover is grooved to provide routing paths for fibres to the outside of the tray and

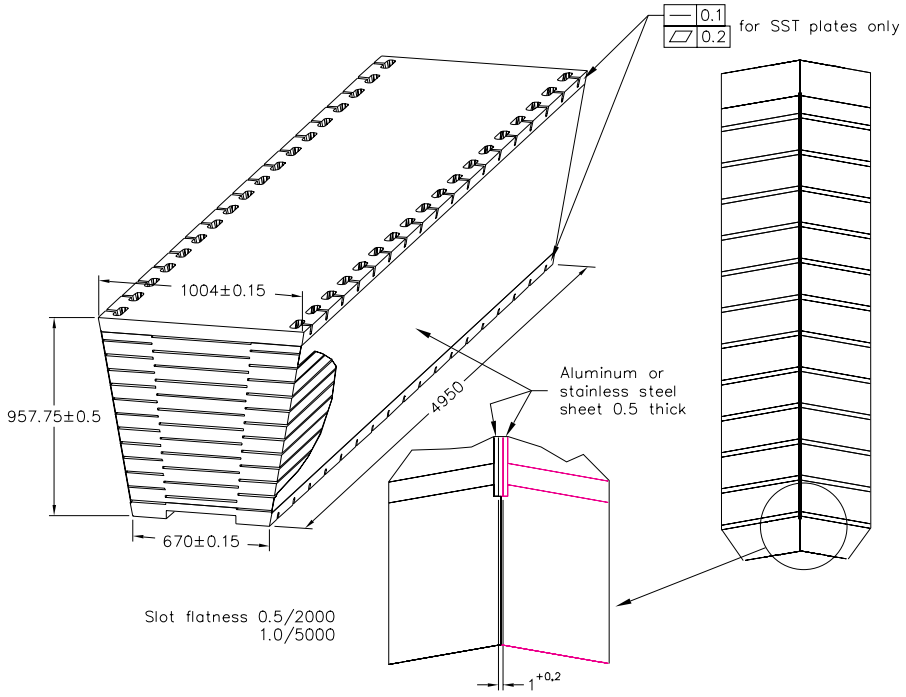

Figure 5.4: Isometric view of the HB wedges, showing the hermetic design of the scintillator sampling.

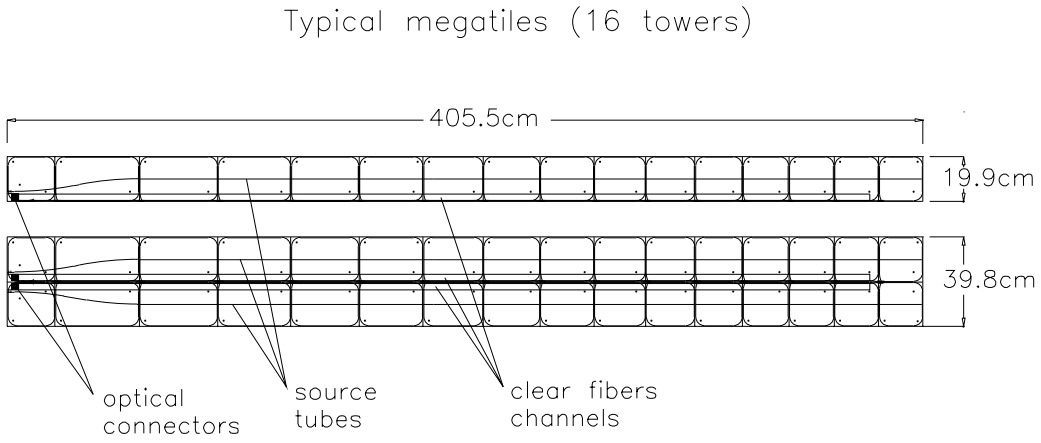

Figure 5.5: Scintillator trays.

also to accommodate the tubes for moving radioactive sources.

After exiting the scintillator, the wavelength shifting fibres (WLS) are spliced to clear fibres (Kuraray double-clad). The clear fibre goes to an optical connector at the end of the tray. An optical cable takes the light to an optical decoding unit (ODU). The ODU arranges the fibres into read-out towers and brings the light to a hybrid photodiode (HPD) [109]. An additional fibre enters each

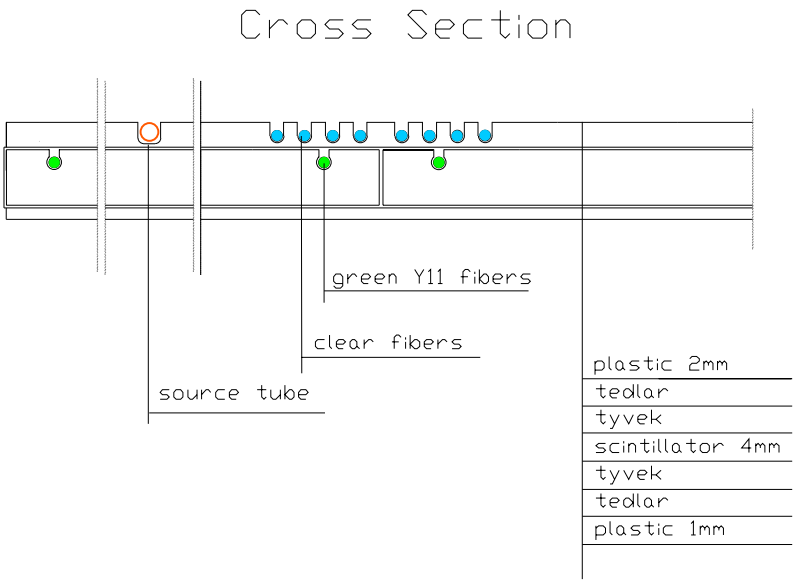

Figure 5.6: Cross-sectional view of a scintillator tray.

Table 5.3: Scintillator in the HB wedges.

layer	*material*	*thickness*
0	Bicron BC408	9 mm
1-15	Kuraray SCSN81	3.7 mm
16	Kuraray SCSN81	9 mm

HPD for direct injection of light using either the laser or a light emitting diode (LED). A schematic of the fibre optics is shown in figure 5.7 and the actual cabling is shown in figure 5.8.

The HPD consists of a photocathode held at a HV of -8 kV at a distance of approximately 3.3 mm from a pixelated silicon photodiode. The ionization produced by the accelerated photo-electron in the diode results in a gain of the HPD of approximately 2000. There are 19 hexagonal 20-mm^2 pixels in a single HPD, the centermost of which is not read-out. A cross sectional view of an HPD is shown in figure 5.9.

During the production and assembly process, the WLS fibres are cut, polished, and mirrored. The reflectivity of the mirror is checked by measuring test fibres which are mirrored along with the fibres used in the calorimeter. Measuring the reflectivity of the mirror is done with a computer controlled UV scanner with the fibres read out by photodiodes. Clear fibres are spliced onto WLS fibres with a fusion splicer. The transmission across the splice is checked by splicing a sample of WLS fibres onto WLS fibres. The splice region is measured with the UV scanner. The transmission across the splice is 92.6% with an RMS of 1.8%. Next, the optical fibres are glued into a 10 fibre connector. This configuration is called a pigtail. In order to get the fibre lengths correct, the pigtail is assembled in a template. The connector is diamond polished. The fibres are measured with the

2008 JINST 3 S08004

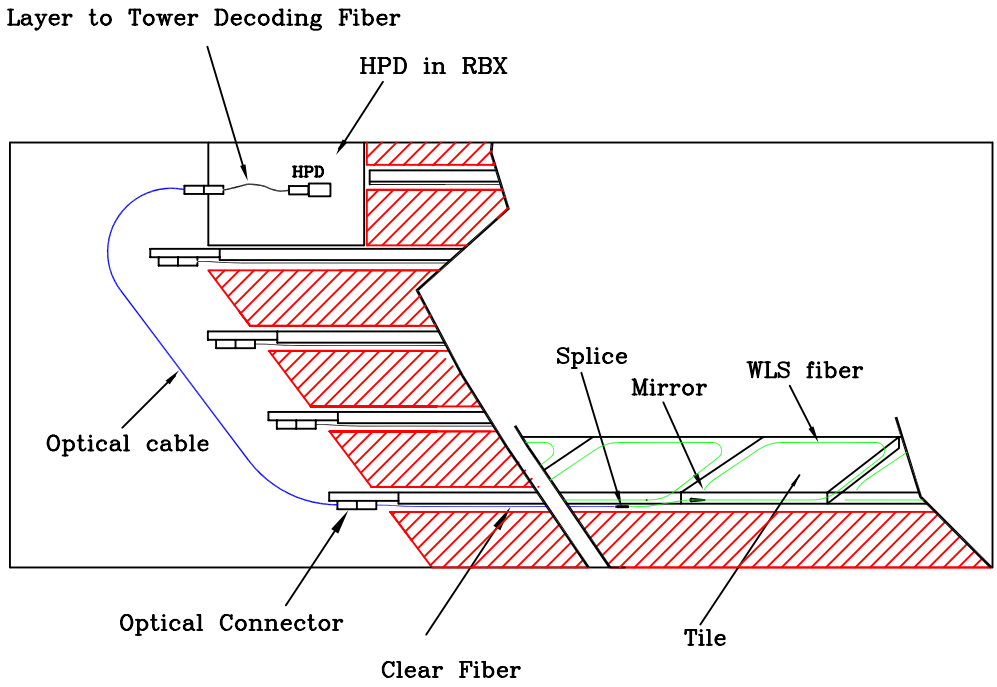

Figure 5.7: Schematic of the HB optics.

UV scanner. The scanner checks the green fibre, clear fibre, splice, and mirror. The RMS of the light from the fibres is 1.9%. After the pigtail is inserted into the tray, the completed tray is checked with an automated source scanner using a Cs^{137} source inside a lead collimator. This yields a 4 cm diameter source spot on the tray. The collimator is moved with a computer controlled x-y motor. From the scanner we determine the relative light yield of each tile and the uniformity of each tray. The light yield of the individual tiles has an RMS of 4.6%, while the transverse uniformity of the tile is 4.5%. A Cs^{137} wire source is run through the 4 source tubes and the light yield is measured. The RMS of the ratio of collimated source to wire source is 1.3%. This means the line sources, which can be used when the calorimeter is completely assembled, can calibrate individual tiles to better than 2%. In addition to the moving wire source, there are laser and LED light injection systems.

Longitudinal segmentation

The η towers 1–14 have a single longitudinal read-out. The η towers closest to the endcap transition region (15 and 16) are segmented in depth. The front segment of tower 15 contains either 12 or 13 scintillators, due to the placement of the read-out box and the staggering of the layers (layers 0–11 for the middle two ϕ sectors and 0–12 layers for the outer two ϕ sectors). The rear segment of tower 15 has three scintillators. Tower 16, which is in front of the endcap (HE) has one scintillators in the front segment and seven in the rear. The front segment of tower 16 does not have a layer-0 scintillator. The tower segmentation is summarized in figure 5.10 and table 5.4.

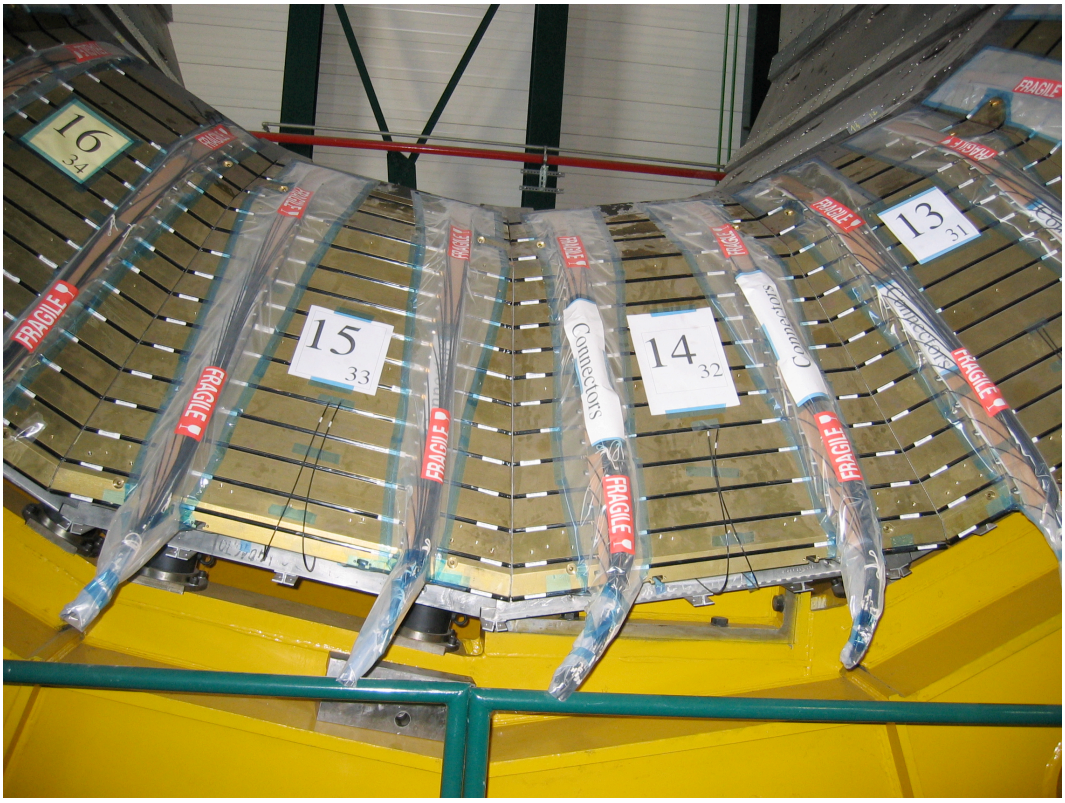

Figure 5.8: Close up view of the assembled HB wedges, showing the optical cabling.

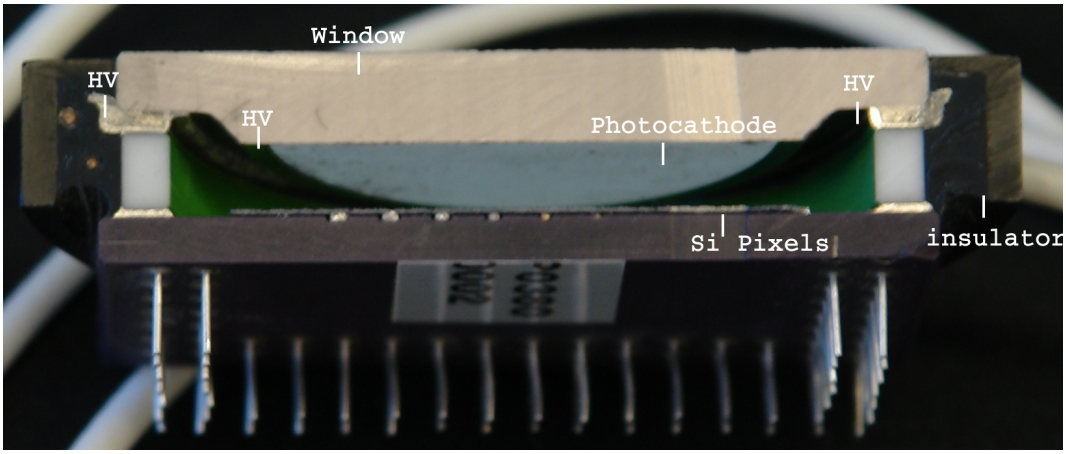

Figure 5.9: Cross sectional view of an HPD.

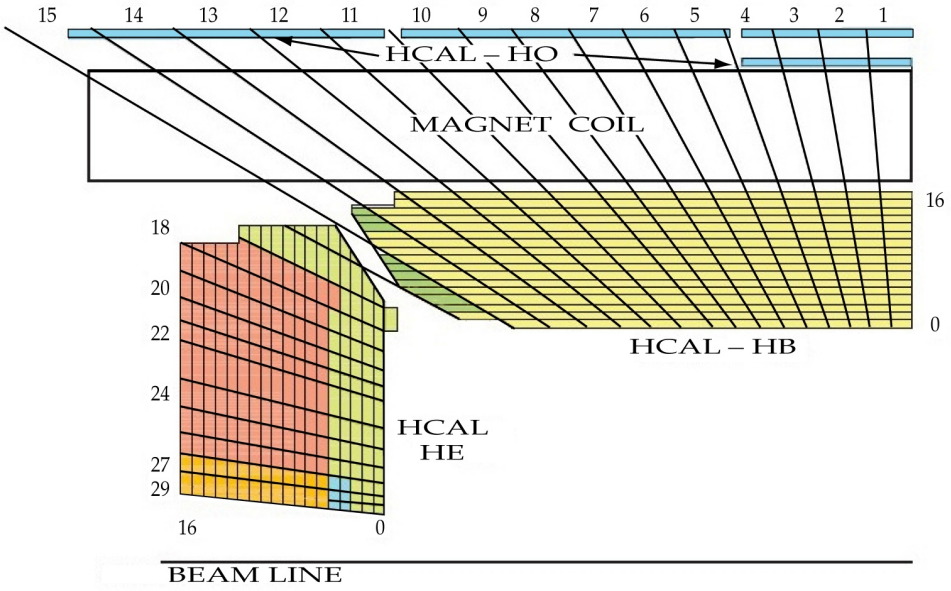

Figure 5.10: The HCAL tower segmentation in the r,z plane for one-fourth of the HB, HO, and HE detectors. The shading represents the optical grouping of scintillator layers into different longitudinal readouts.

Table 5.4: Tower data for HB. The given thicknesses correspond to the center of the tower. Note that tower 16 overlaps with HE.

tower	η *range*	*thickness* (λ_I)
1	0.000 – 0.087	5.39
2	0.087 – 0.174	5.43
3	0.174 – 0.261	5.51
4	0.261 – 0.348	5.63
5	0.348 – 0.435	5.80
6	0.435 – 0.522	6.01
7	0.522 – 0.609	6.26
8	0.609 – 0.696	6.57
9	0.696 – 0.783	6.92
10	0.783 – 0.870	7.32
11	0.870 – 0.957	7.79
12	0.957 – 1.044	8.30
13	1.044 – 1.131	8.89
14	1.131 – 1.218	9.54
15	1.218 – 1.305	10.3
16	1.305 – 1.392	overlaps with HE

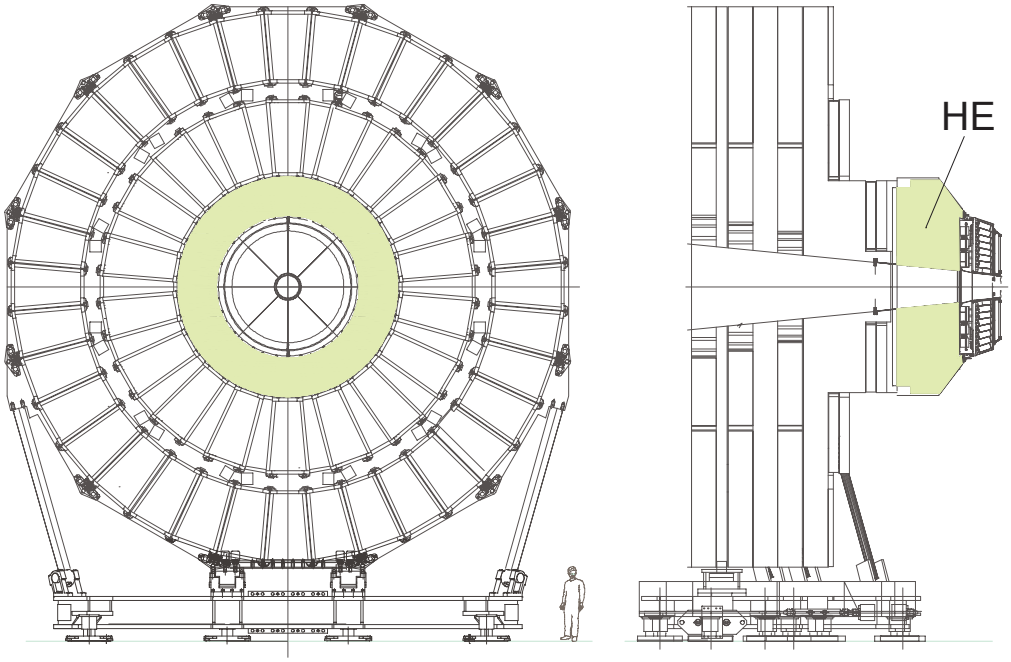

Figure 5.11: Hadron endcap (HE) calorimeter mounted on the endcap iron yoke.

5.2 Endcap design (HE)

The hadron calorimeter endcaps (HE) [108] cover a substantial portion of the rapidity range, $1.3 < |\eta| < 3$ (13.2% of the solid angle), a region containing about 34% of the particles produced in the final state. The high luminosity of the LHC (10^{34} cm^{-2} s^{-1}) requires HE to handle high (MHz) counting rates and have high radiation tolerance (10 MRad after 10 years of operation at design luminosity) at $|\eta| \simeq 3$. Since the calorimeter is inserted into the ends of a 4-T solenoidal magnet, the absorber must be made from a non-magnetic material. It must also have a maximum number of interaction lengths to contain hadronic showers, good mechanical properties and reasonable cost, leading to the choice of C26000 cartridge brass. The endcaps are attached to the muon endcap yoke as shown in figures 5.11 and 5.12. Only a small part of the calorimeter structure can be used for the fixation to the magnet iron, because the majority of the space between HE and muon absorber is occupied with muon cathode strip chambers. A 10-t electromagnetic calorimeter (EE) with a 2-t preshower detector (ES) is attached at the front face of HE. The large weight involved (about 300 t) and a strict requirement to minimize non-instrumented materials along particle trajectories, has made the design of HE a challenge to engineers. An interface kinematic scheme was developed in order to provide precise positioning of the endcap detectors with respect to the adjacent muon station, and to minimize the influence of deformation under magnetic forces. The interface kinematic contains a sliding joint between the interface tube, and HE back-flange and the hinge connection between brackets and the iron disk (YE1). Structural materials used in the interface system are non-magnetic in order not to distort the axial magnetic field of up to 4 T.

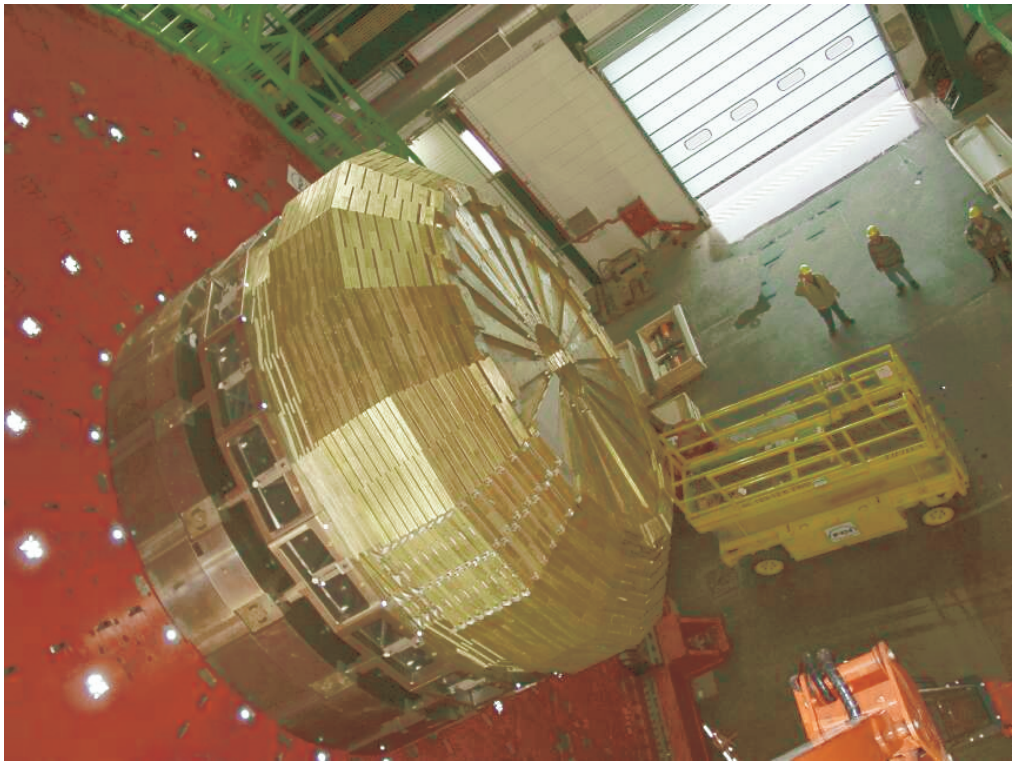

Figure 5.12: Partially assembled HE-minus absorber in the CMS surface hall (SX5). Scintillator trays can be seen to be inserted in some of the outer sectors.

Absorber geometry

The design of the absorber is driven by the need to minimize the cracks between HB and HE, rather than single-particle energy resolution, since the resolution of jets in HE will be limited by pileup, magnetic field effects, and parton fragmentation [110, 111]. The plates are bolted together in a staggered geometry resulting in a configuration that contains no projective "dead" material (figure 5.13). The design provides a self-supporting hermetic construction. The brass plates are 79-mm-thick with 9-mm gaps to accommodate the scintillators. The total length of the calorimeter, including electromagnetic crystals, is about 10 interaction lengths (λ_I).

The outer layers of HE have a cutout region for installation of the photodetectors and front-end electronics. To compensate for the resulting reduction of material, an extra layer (-1) is added to tower 18 [112]. The outer layers are fixed to a 10-cm-thick stainless steel support plate. The optical elements are inserted into the gaps after the absorber is completely assembled; therefore, the optical elements must have a rigid structure to allow insertion from any position.

Scintillator trays

The scintillation light is collected by wavelength shifting (WLS) fibres [113, 114]. The design minimizes dead zones because the absorber can be made as a solid piece without supporting structures while at the same time the light can be easily routed to the photodetectors. Trapezoidal-

2008 JINST 3 S08004

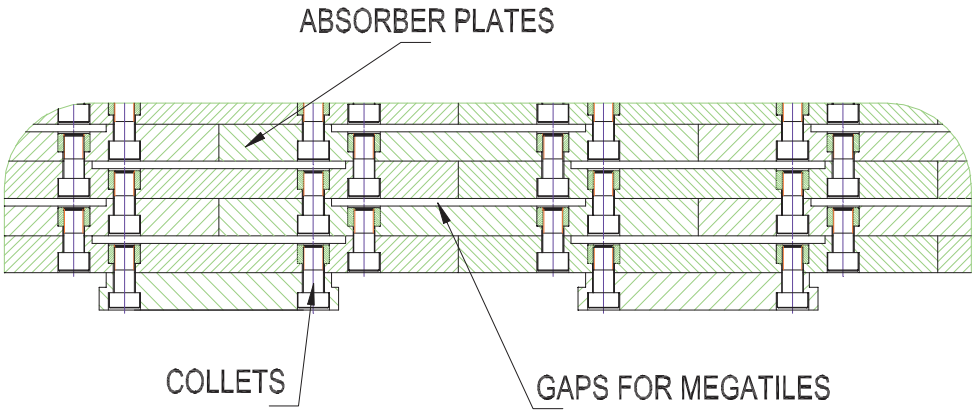

Figure 5.13: Mechanical structure of the HE absorber. Particles enter the calorimeter from the bottom.

shaped scintillators (figure 5.14), 3.7-mm-thick SCSN81 for layers 1–17 and 9-mm-thick Bicron BC408 for layer 0, have grooves in which the WLS fibres are inserted. The ends of the fibres are machined with a diamond fly cutter and one end is covered with aluminium to increase the light collection. The other end is spliced to a clear fibre, which is terminated in an optical connector. The connector with the glued fibres is also machined by a diamond fly cutter. The scintillator is painted along the narrow edges and put into a frame to form a tray. The total number of tiles for both HE calorimeters is 20 916 and the number of trays is 1368. The design of a tray is presented in figure 5.15. The numbering scheme in η is shown in figure 5.16, and the CMS convention for ϕ as applied to HE is shown in figure 5.17. The scintillators are wrapped with Tyvek and sandwiched between sheets of duraluminum. The stack contains holes for fibres which are terminated with optical connectors. The gap between the duraluminum plates is fixed by brass spacers screwed together. The granularity of the calorimeters is $\Delta\eta \times \Delta\phi = 0.087 \times 0.087$ for $|\eta| < 1.6$ and $\Delta\eta \times \Delta\phi \approx 0.17 \times 0.17$ for $|\eta| \geq 1.6$.

The tray design is very robust and reliable. The trays are relatively stiff which is very important for insertion into the absorber. To control the scintillator tray quality, a UV nitrogen laser was used to excite the scintillators. The light is fed by quartz fibres to the connector and is fanned out as shown in figure 5.15. These fibres are terminated with aluminium reflectors and distribute the light to all tiles. The light signal produced by a UV flash in the scintillator is similar to the signal induced by a charged particle. This allows a performance check of the entire optical route from scintillator to electronics, providing an important technique to track possible degradation of transparency due to radiation damage. For further calibration and monitoring, a radioactive source moving in a stainless steel tube is used to study the time-dependence of calibration coefficients.

The trays are inserted into the gaps in the absorber and fixed by screws. At the back of the calorimeter, boxes with photodetectors and electronics are located in the notch shown in figure 5.18. Optical cables transfer signals from the scintillator trays to the photodetectors. The partially assembled HE is shown in figure 5.12. Multipixel hybrid photodiodes (HPDs) are used as photodetectors due to their low sensitivity to magnetic fields and their large dynamical range.

2008 JINST 3 S08004

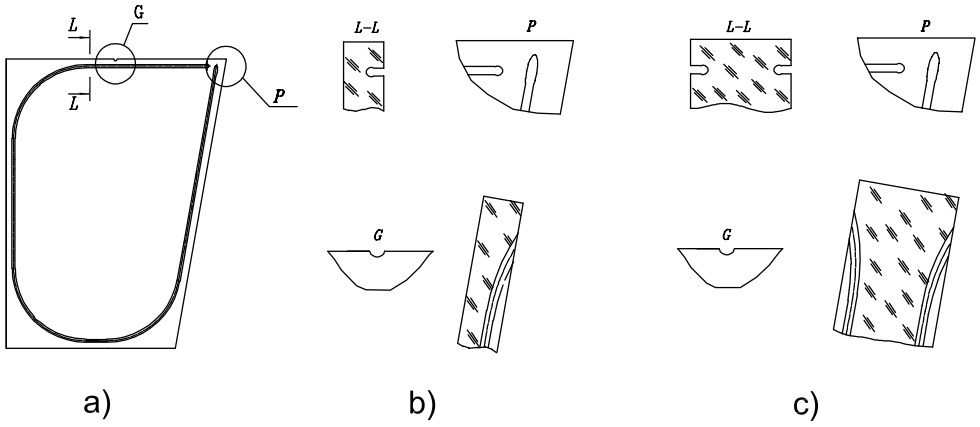

Figure 5.14: a) Basic structure of a scintillator tile with a groove to fix wavelength shifting fibre, b) cross section of the 3.7-mm-thick scintillator for layers 1–17, and c) cross section of the 9-mm-thick scintillator for layer zero. Two layers of reflecting paint cover the side surfaces of the tile.

Longitudinal segmentation

The longitudinal segmentation of HE (figure 5.10) is, in part, motivated by the radiation environment. Correction of the calibration coefficients after scintillator degradation can be applied, in order to restore the energy resolution. The towers nearest the beam line (27 and 28 plus guard ring "29") have 3 divisions in depth which are read-out separately. The other towers (except 16 and 17 which overlap with the electromagnetic barrel calorimeter) have two longitudinal readouts for potential use during the time period when the electromagnetic endcap calorimeter (EE) may not yet be available. A special scintillator layer of 9 mm BC408 (layer 0) is installed in front of the absorber to partially correct for the different response of EE to electrons and hadrons and for particle absorption in the mechanical structure supporting EE.

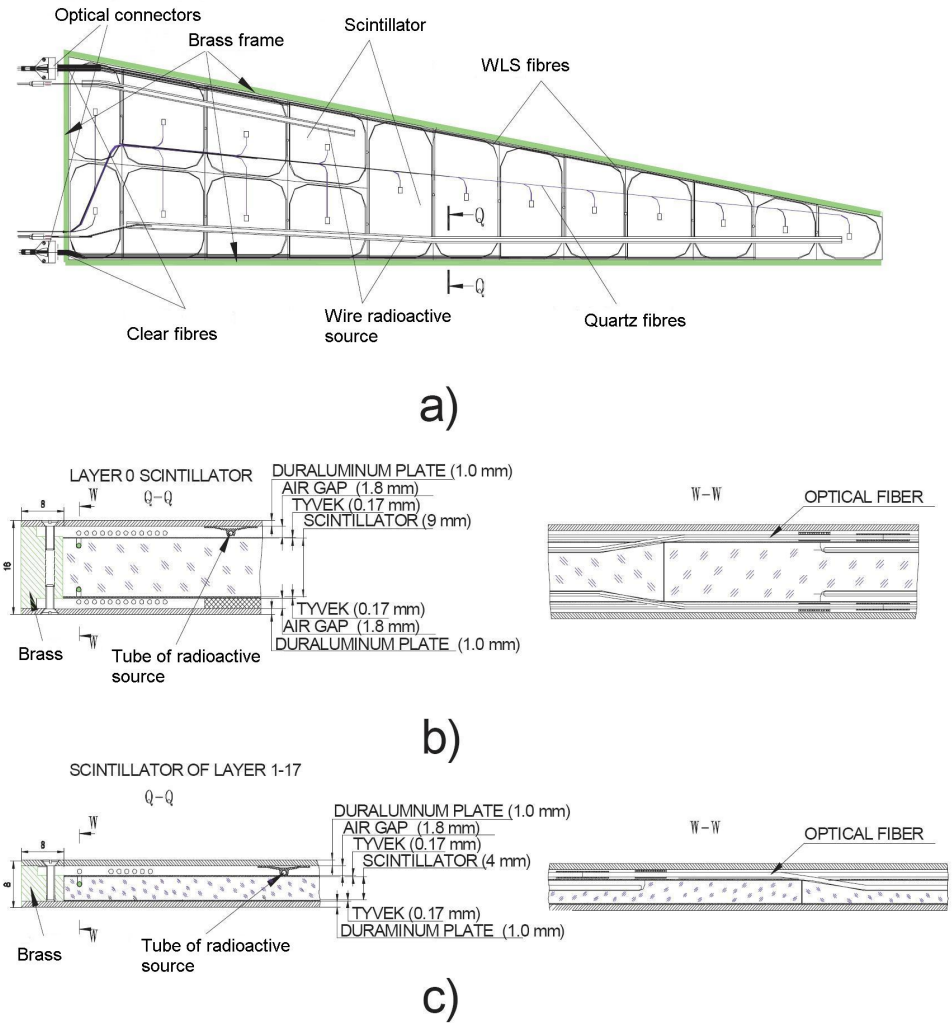

Figure 5.15: The design of the calorimeter scintillator trays: a) front view of a tray without upper aluminium cover, b) cut out view of the layer-0 tray with two fibres from a tile, c) cut out view of a tray for layers 1–17.

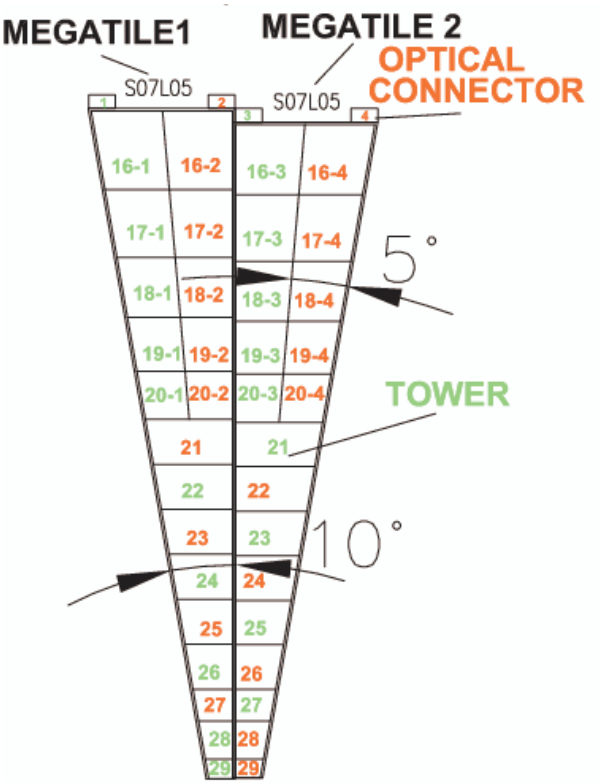

Figure 5.16: Numbering scheme for the tiles in adjacent scintillator trays.

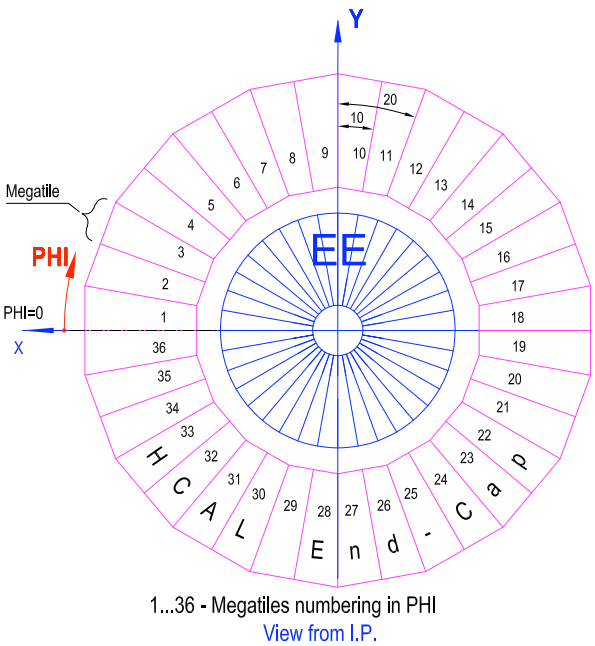

Figure 5.17: Numbering scheme for the HE wedges as viewed from the interaction point. The $+x$ direction points to the center of the LHC ring.

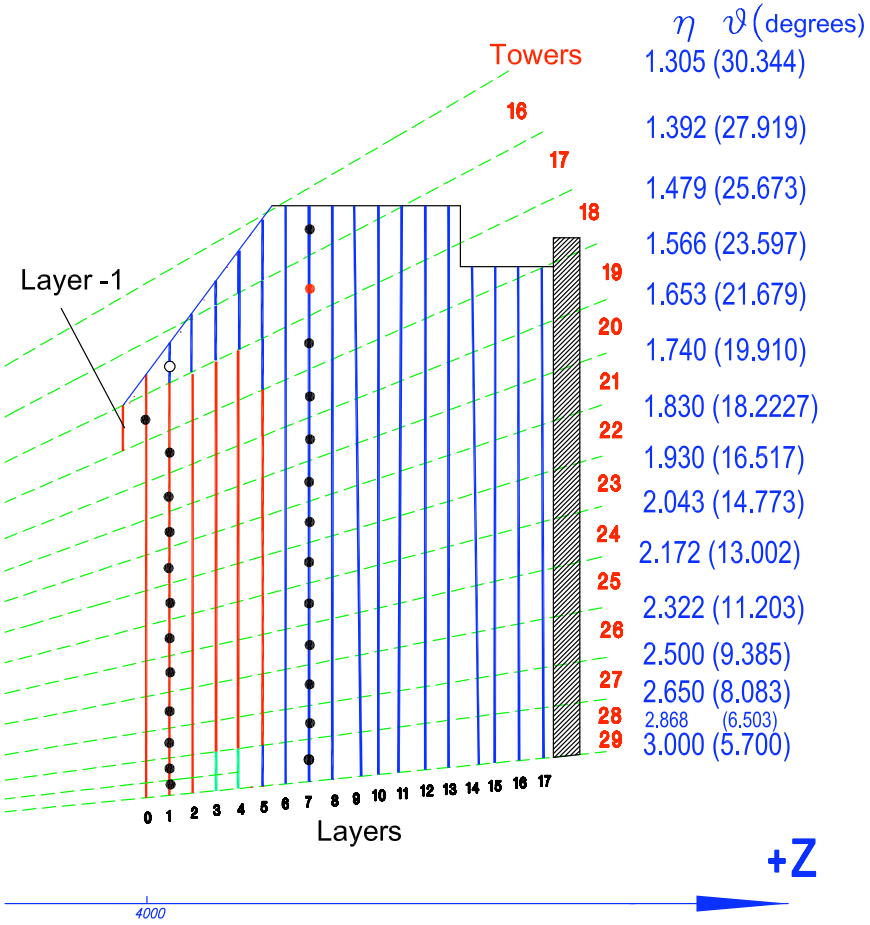

Figure 5.18: Longitudinal and angular segmentation of the HE calorimeter. The dashed lines point to the interaction point.

2008 JINST 3 S08004

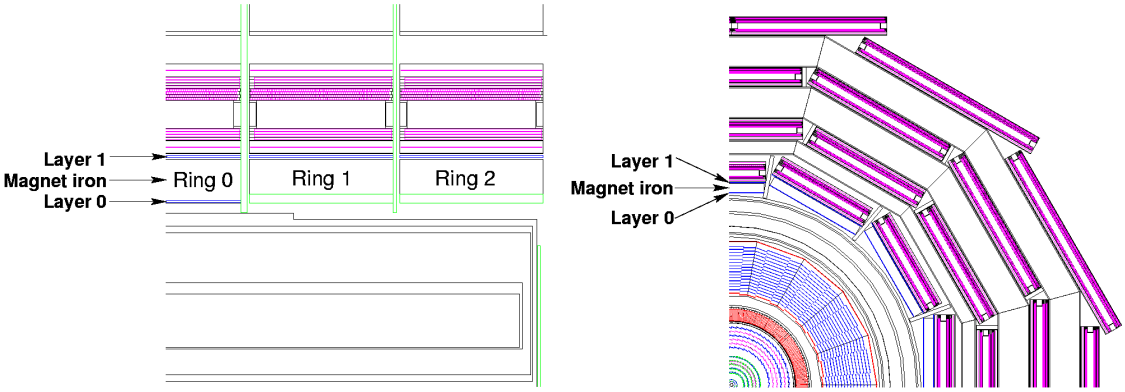

Figure 5.19: Longitudinal and transverse views of the CMS detector showing the position of HO layers.

5.3 Outer calorimeter design (HO)

In the central pseudorapidity region, the combined stopping power of EB plus HB does not provide sufficient containment for hadron showers. To ensure adequate sampling depth for $|\eta| < 1.3$, the hadron calorimeter is extended outside the solenoid with a tail catcher called the HO or outer calorimeter. The HO utilises the solenoid coil as an additional absorber equal to $1.4/\sin\theta$ interaction lengths and is used to identify late starting showers and to measure the shower energy deposited after HB.

Outside the vacuum tank of the solenoid, the magnetic field is returned through an iron yoke designed in the form of five 2.536 m wide (along z-axis) rings. The HO is placed as the first sensitive layer in each of these five rings. The rings are identified by the numbers -2, -1, 0, $+1$, $+2$. The numbering increases with z and the nominal central z positions of the five rings are respectively -5.342 m, -2.686 m, 0, $+2.686$ m and $+5.342$ m. At $\eta = 0$, HB has the minimal absorber depth. Therefore, the central ring (ring 0) has two layers of HO scintillators on either side of a 19.5 cm thick piece of iron (the tail catcher iron) at radial distances of 3.82 m and 4.07 m, respectively. All other rings have a single HO layer at a radial distance of 4.07 m. The total depth of the calorimeter system is thus extended to a minimum of 11.8 λ_I except at the barrel-endcap boundary region.

The HO is constrained by the geometry of the muon system. Figure 5.19 shows the position of HO layers in the rings of the muon stations in the overall CMS setup. The segmentation of these detectors closely follows that of the barrel muon system. Each ring has 12 identical ϕ-sectors. The 12 sectors are separated by 75-mm-thick stainless steel beams which hold successive layers of iron of the return yoke as well as the muon system. The space between successive muon rings in the η direction and also the space occupied by the stainless steel beams in the ϕ direction are not available for HO. In addition, the space occupied by the cryogenic "chimneys" in sector 3 of ring -1, and sector 4 of ring $+1$ are also not available for HO. The chimneys are used for the cryogenic transfer lines and power cables of the magnet system. Finally, the mechanical structures needed to position the scintillator trays further constrain HO along ϕ.

2008 JINST 3 S08004

In the radial direction each HO layer has been allocated a total of 40 mm, of which only 16 mm is available for the detector layer, the rest being used for the aluminium honeycomb support structures. In addition, the HO modules are independently supported from the steel beams located on either side of each ϕ sector. The thickness and position of the iron ribs in the yoke structure further constrain the shape and segmentation of the HO.

The sizes and positions of the tiles in HO are supposed to roughly map the layers of HB to make towers of granularity $0.087\times$ 0.087 in η and ϕ. The HO consists of one (rings ±1 and ±2) or two (ring 0) layers of scintillator tiles located in front of the first layer of the barrel muon detector. Scintillation light from the tiles is collected using multi-clad Y11 Kuraray wavelength shifting (WLS) fibres of diameter 0.94 mm, and transported to the photo detectors located on the structure of the return yoke by splicing a multi-clad Kuraray clear fibre (also of 0.94 mm diameter) with the WLS fibre. In order to simplify installation of HO, the scintillator tiles are packed into a single unit called a tray. Each tray corresponds to one ϕ slice (5° wide in ϕ). However, along the z (η) direction, a tray covers the entire span of a muon ring. Figure 5.20 shows a schematic view of a HO tray where one tile is mapped to a tower of HB and the optical cable from the tray is connected to the read-out box.

The physics impact of HO has been studied [115] using a simulation of the CMS detector. Single pions of fixed energies are shot at specific η values and the resulting energy deposits in the electromagnetic calorimeter and in the layers of the hadron calorimeter are combined to measure the energy. Figure 5.21 shows distributions of the measured energy scaled to the incident energy for 200 GeV pions at η = 0 and 225 GeV at η = 0.5 (pointing towards the middle of ring 1). The solid and dashed lines in the figure indicate measurements without and with HO, respectively. As can be seen in figure 5.21, there is an excess in $\mathrm{Energy/E_{incident}} < 1$ for measurements without HO, because of leakage. The measurements with HO are more Gaussian in nature indicating that the addition of HO recovers the effect of leakage. The effect of leakage is visible at η = 0 (ring 0) from 70 GeV, increasing with energy. The mean fraction of energy in HO increases from 0.38% for 10 GeV pions to 4.3% for 300 GeV pions. There is some evidence of leakage without HO in ring 1 but it is reduced due to the greater HB thickness at larger $|\eta|$. The amount of leakage in ring 2 is found to be negligible at energies below 300 GeV.

The effect of shower leakage has a direct consequence on the measurement of missing transverse energy (E_T^{miss}). Study of QCD events shows that the cross section for those events, where at least one particle has E_T above 500 GeV, is several pb. For these events the HO is useful to decrease the leakage and improve the E_T^{miss} measurement. Figure 5.22 shows the dijet integrated cross section for E_T^{miss} above a certain value. It is clear from the figure that the inclusion of HO reduces the dijet rate by a factor of 1.5 or more for moderate E_T^{miss} values, a region important for searches of supersymmetric particles.

Module specification

HO is physically divided into 5 rings in η conforming to the muon ring structure. The rings are numbered $-2, -1, 0, +1$ and $+2$ with increasing η. Each ring of the HO is divided into 12 identical ϕ sectors and each sector has 6 slices (numbered 1 to 6 counting clockwise) in ϕ. The ϕ slices of a layer are identical in all sectors. The widths of the slices along ϕ are given in table 5.5. In each ϕ

2008 JINST 3 S08004

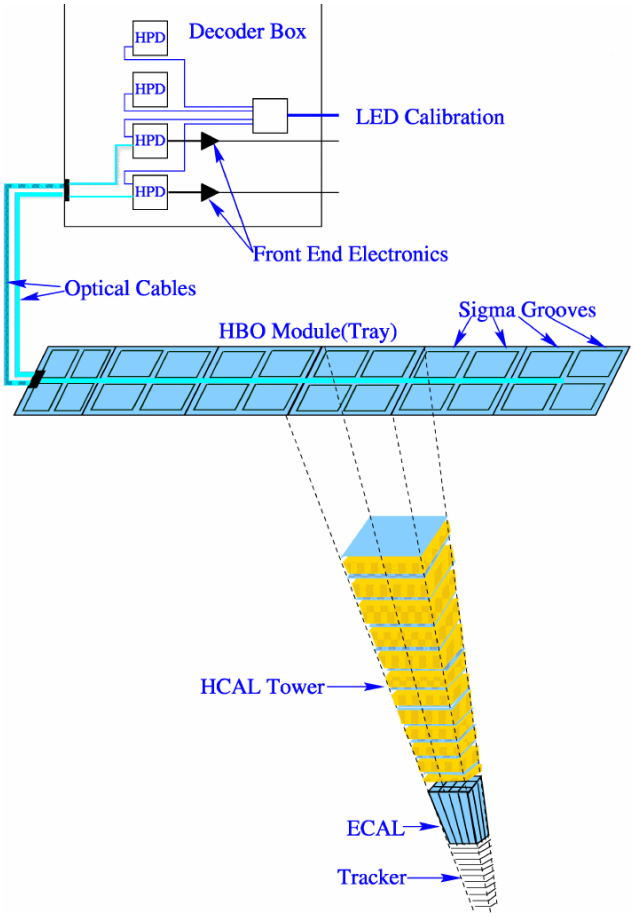

Figure 5.20: Schematic view of a HO tray shown with individual tiles and the corresponding grooves for WLS fibres. Each optically independent (4 WLS fibres) tile is mapped to a tower of HB. Optical fibres from the tray are routed to the decoder box which contains the photodetector and read-out electronics.

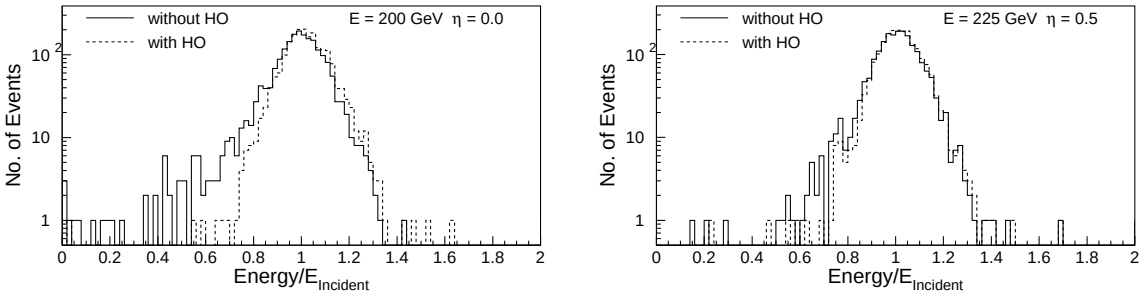

Figure 5.21: A simulation of the distribution of the measured energy scaled to the incident energy for pions with incident energies of (left panel) 200 GeV at $\eta = 0$ and (right panel) 225 GeV at $|\eta| = 0.5$. The solid and dashed histograms are measurements without and with HO, respectively.

2008 JINST 3 S08004

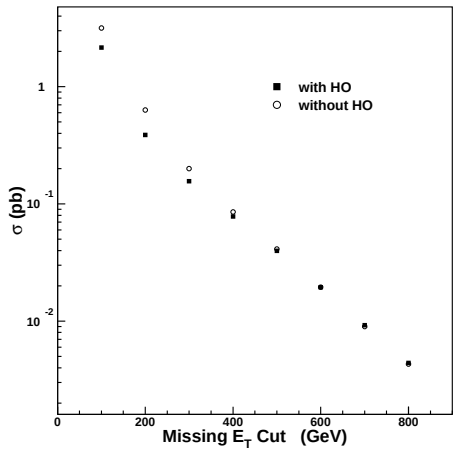

Figure 5.22: Integrated cross section above threshold for intrinsically balanced QCD dijet events as a function of missing E_{T} with or without HO.

Table 5.5: Dimension of tiles along ϕ for different trays. Each tray corresponds to one ϕ-slice in a ϕ sector.

Ring	Layer	Width along ϕ in mm					
		Tray 1	Tray 2	Tray 3	Tray 4	Tray 5	Tray 6
0	0	274	343	332	327	327	268
0	1	300	364	352	347	347	292
±1, ±2	1	317	366	354	349	349	406

slice, there is a further division along η. The smallest scintillator unit in HO thus obtained is called a tile. The scintillator tiles in each ϕ sector belong to a plane. The perpendicular distance of this plane from the z-axis is 3.82 m for layer 0 and 4.07 m for layer 1. The tiles in each ϕ slice of a ring are mechanically held together in the form of a tray.

Both layers of ring 0 have 8 η-divisions (i.e. 8 tiles in a tray): -4, -3, -2, -1, $+1$, $+2$, $+3$, $+4$. Ring 1 has 6 divisions: $5\cdots10$ and ring 2 has 5 divisions: $11\cdots15$. Ring -1 and ring -2 have the same number of divisions as rings 1 and 2 but with $-$ve indices. The η-dimension of any tile with $-$ve tower number is the same as the one with $+$ve number. The tile dimensions along η are shown in table 5.6.

Figure 5.23 shows the final layout of all the HO trays in the CMS detector. The length of a full tray is 2510 mm whereas the shorter trays, the sizes of which are constrained because of the chimney (trays 4 and 5 in sector 4 of ring $+1$ and trays 3, 4, 5 and 6 in sector 3 of ring -1), are 2119-mm long. The shorter trays are constructed without the tile corresponding to tower number ±5. Because of the constraints imposed by the gap between ring 0 and rings ±1, the η boundaries of HO tower 4 do not match the barrel η boundaries; therefore, part of HO tower 5 overlaps with tower 4 in the barrel.

Table 5.6: HO tile dimensions along η for different rings and layers. The tile sizes, which are constrained by muon ring boundaries, are also given.

Tower #	η_{max}	Length (mm)	Tower #	η_{max}	Length (mm)
Ring 0 Layer 0			Ring 0 Layer 1		
1	0.087	331.5	1	0.087	351.2
2	0.174	334.0	2	0.174	353.8
3	0.262	339.0	3	0.262	359.2
4	0.326	248.8	4	0.307	189.1
Ring 1 Layer 1			Ring 2 Layer 1		
5	0.436	391.5	11	0.960	420.1
6	0.524	394.2	12	1.047	545.1
7	0.611	411.0	13	1.135	583.3
8	0.698	430.9	14	1.222	626.0
9	0.785	454.0	15	1.262	333.5
10	0.861	426.0			

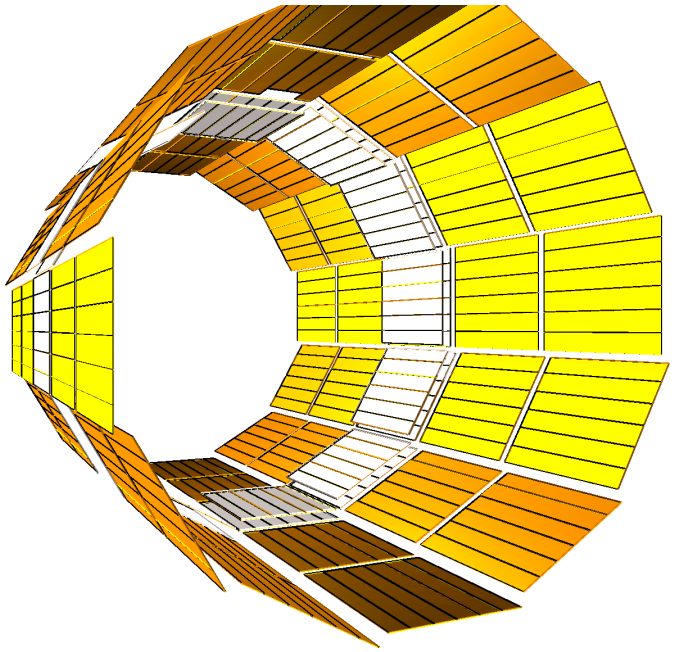

Figure 5.23: Layout of all the HO trays in the CMS detector.

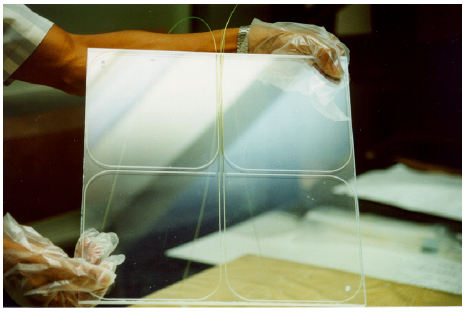

Figure 5.24: View of a typical tile of HO with WLS fibres inserted in the 4 grooves of the tile.

Tiles

Scintillator tiles are made from Bicron BC408 scintillator plates of thickness 10^{+0}_{-1} mm. Figure 5.24 shows a typical HO scintillator tile. The WLS fibres are held inside the tile in grooves with a key hole cross section. Each groove has a circular part (of diameter 1.35 mm) inside the scintillator and a neck of 0.86 mm width. The grooves are 2.05-mm deep. Each tile has 4 identical grooves, one groove in each quadrant of the tile. The grooves closely follow the quadrant boundary. The corners of the grooves are rounded to prevent damage to the fibre at the bend and to ease fibre insertion. The groove design is slightly different for the tile where the optical connector is placed at the end of the tray. Since the tiles are large, 4 grooves ensure good light collection and less attenuation of light.

The HO has 95 different tile dimensions, 75 for layer 1 and 20 for layer 0. The total number of tiles is 2730 (2154 for layer 1 and 576 for layer 0).

Trays

All tiles in each ϕ slice of a sector are grouped together in the form of a tray. Each tray contains 5 tiles in rings ± 2; 6 tiles in rings ± 1 and 8 tiles in ring 0. The edges of the tiles are painted with Bicron reflecting white paint for better light collection as well as isolating the individual tiles of a tray. Further isolation of tiles is achieved by inserting a piece of black tedler in between the adjacent tiles. The tiles in a tray are covered with a single big piece of white, reflective tyvek paper. Then they are covered with black tedlar paper to prevent light leakage. This package is placed between two black plastic plates for mechanical stability and ease of handling. The top plastic cover is 2-mm-thick and the bottom one is 1-mm-thick. Figure 5.25 shows a cross section of a tray to illustrate the different components. The plastic covers (top and bottom) have holes matching with the holes in the tiles. Specially designed countersunk screws passing through these holes fix the plastic covers firmly on the tiles.

The 2 mm plastic sheet on the top has 1.6 mm deep channels grooved on it (on the outer side) to route the fibres from individual tiles to an optical connector placed in a groove at the edge of the tray. A 1.5-mm-wide straight groove runs along the edge of the top cover to accommodate a stainless steel tube. This is used for the passage of a radioactive source which is employed in calibrating the modules. Each connector has two holes and they are fixed to the scintillator-plastic assembly through matching holes. Each ϕ sector in each ring has 6 trays. There are 360 trays for layer 1 and 72 trays for layer 0.

2008 JINST 3 S08004

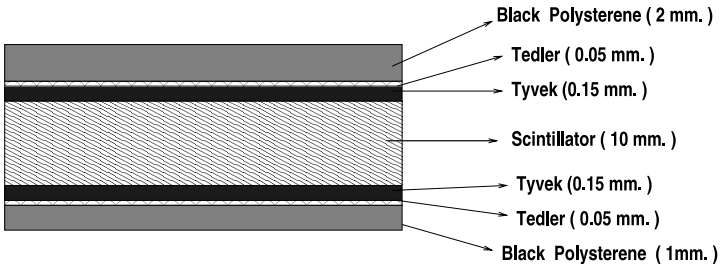

Figure 5.25: Cross section of a HO tray showing the different components.

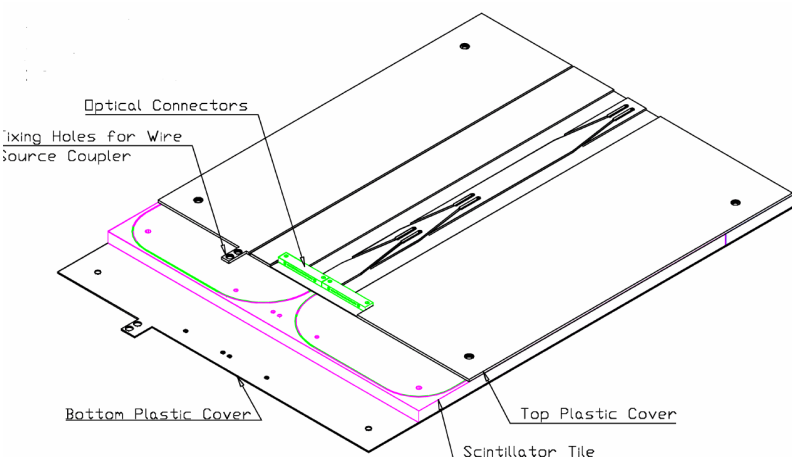

Figure 5.26: The arrangement of scintillation tiles, plastic covers and connectors in a tray. The components are slightly displaced from their true positions to show their matching designs.

Pigtails

The light collected by the WLS fibres inserted in the tiles needs to be transported to photodetectors located far away on the muon rings. The captive ends of the WLS fibres, which reside inside the groove, are polished, aluminized and protected using a thin polymer coating. The other end of the WLS fibre comes out of the tile through a slot made on the 2-mm-thick black plastic cover sheet. To minimise the loss of light in transportation, the WLS fibre (attenuation length of $\approx$ 1.8 m) is spliced to a clear fibre (attenuation length of $\approx$ 8.0 m). A fibre is spliced only if the potential WLS light loss is larger than the light loss at a spliced joint. Thus depending on tile length (along η) 2–3 fibres in each pigtail are made only of WLS fibres. The clear fibres from each tile follow the guiding grooves on the top plastic to the optical connector at the end. Each tray has two optical connectors mounted on one end of the tray. In a tray, the grooves of the tiles form two rows along η. The fibres from all grooves on one row terminate on one connector (figure 5.26). The number of fibres from trays in different rings are given in table 5.7.

The bunch of fibres fixed to the optical connector is called a pigtail (figure 5.27). Each tray has 2 pigtails and there are 864 pigtails in total: 720 for layer 1 and 144 for layer 0. Each fibre in a pigtail is cut to the proper length to match the groove length in the scintillator plus the distance from the scintillator to the optical connector at the end of the tray.

Table 5.7: Tray specifications for different rings of HO.

Ring #	Tiles/tray	Fibres/tray	Fibres/connector
0	8	32	16
± 1	6	24	12
± 2	5	20	10

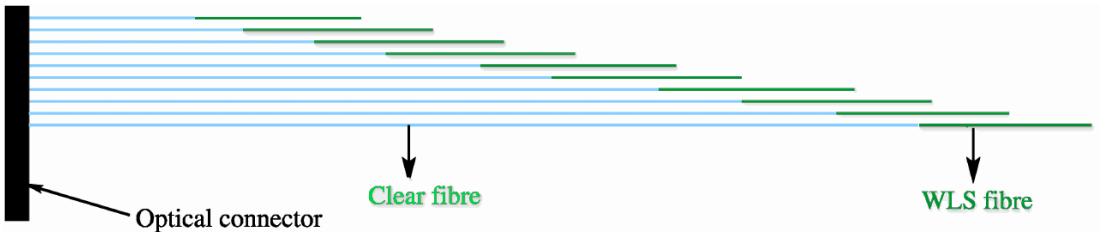

Figure 5.27: Illustration of an assembled pigtail (not drawn to scale).

5.4 Forward calorimeter design (HF)

The forward calorimeter will experience unprecedented particle fluxes. On average, 760 GeV per proton-proton interaction is deposited into the two forward calorimeters, compared to only 100 GeV for the rest of the detector. Moreover, this energy is not uniformly distributed but has a pronounced maximum at the highest rapidities. At $|\eta| = 5$ after an integrated luminosity of $5 \times 10^5\,\mathrm{pb}^{-1}$ (≈ 10 years of LHC operation), the HF will experience ≈ 10 MGy. The charged hadron rates will also be extremely high. For the same integrated luminosity, inside the HF absorber at 125 cm from the beam-line, the rate will exceed 10^{11} per cm^2 [108]. This hostile environment presents a considerable challenge to calorimetry, and the design of the HF calorimeter was first and foremost guided by the necessity to survive in these harsh conditions, preferably for at least a decade. Successful operation critically depends on the radiation hardness of the active material. This was the principal reason why quartz fibres (fused-silica core and polymer hard-cladding) were chosen as the active medium.

The signal is generated when charged shower particles above the Cherenkov threshold ($E \geq 190$ keV for electrons) generate Cherenkov light, thereby rendering the calorimeter mostly sensitive to the electromagnetic component of showers [116]. A small fraction of the generated light is captured, $f_{\mathrm{trap}} = \mathrm{NA}/2n_{\mathrm{core}}^2$, where NA is the numerical aperture ($\mathrm{NA} = 0.33 \pm 0.02$) and n_{core} is the refractive index of the quartz core. Only light that hits the core-cladding interface at an angle larger than the critical angle (71°) contributes to the calorimeter signal. The half-angle $\theta = 19°$ is determined by the refractive indices of the core (n_{core}) and the cladding (n_{clad}), $\sin\theta = \sqrt{n_{\mathrm{core}}^2 - n_{\mathrm{clad}}^2}$. The fibres measure 600 ± 10 μm in diameter for the fused-silica core, 630^{+5}_{-10} μm with the polymer hard-cladding, and 800 ± 30 μm with the protective acrylate buffer. Over 1000 km of fibres are used in the HF calorimeters. The fibres are cleaved at both ends by a diamond cutter. The attenuation length of these fibres is measured to be $\approx$15 m using high energy electrons at 90° to the fibres.

The optical attenuation at a wavelength λ in these types of fibres scales as $a(\lambda)(D/D_0)^{b(\lambda)}$ where D is the accumulated dose, which is normalized to a reference dose ($D_0 = 1$ MGy) for convenience. For example, at a wavelength $\lambda = 450$ nm at the accumulated dose of $D = 1$ MGy, the induced attenuation is ≈ 1.5 dB/m, thus defining a. The a and b parameters characterize the radiation hardness of a given fibre. For high OH^- (300–500 ppm) HF fibres at 450 nm, the measured values are $a \approx 1.5$ and $b \approx 0.3$ [117–119]. An accumulated dose of 10 MGy will result in a loss of optical transmission by a half, which is the worst case for HF after a decade.

The calorimeter consists of a steel absorber structure that is composed of 5 mm thick grooved plates. Fibres are inserted in these grooves. The detector is functionally subdivided into two longitudinal segments. Half of the fibres run over the full depth of the absorber (165 cm $\approx 10\lambda_I$) while the other half starts at a depth of 22 cm from the front of the detector. These two sets of fibres are read out separately. This arrangement makes it possible to distinguish showers generated by electrons and photons, which deposit a large fraction of their energy in the first 22 cm, from those generated by hadrons, which produce nearly equal signals in both calorimeter segments on average. The long fibre section is referred as L (measuring the total signal), and the short fibre section as S (measuring the energy deposition after 22 cm of steel). The absorber has grooves ($0.90^{+0.12}_{-0}$ mm wide and $1.06^{+0.6}_{-0}$ mm in depth) which make a square grid separated by 5.0 ± 0.1 mm center-to-center. Long and short fibres alternate in these grooves. The packing fraction by volume (fibre/total) in the first 22 cm is 0.57% and is twice as large beyond that depth.

The forward calorimeter is essentially a cylindrical steel structure with an outer radius of 130.0 cm. The front face of the calorimeter is located at 11.2 m from the interaction point. The hole for the beam pipe is cylindrical, with radius 12.5 cm from the center of the beam line. This structure is azimuthally subdivided into 20° modular wedges. Thirty-six such wedges (18 on either side of the interaction point) make up the HF calorimeters. A cross sectional view of the HF is shown in figure 5.28. The fibres run parallel to the beam line, and are bundled to form 0.175×0.175 ($\Delta\eta \times \Delta\phi$) towers (figure 5.29 and table 5.8). The detector is housed in a hermetic radiation shielding which consists of layers of 40 cm thick steel, 40 cm of concrete, and 5 cm of polyethylene. A large plug structure in the back of the detector provides additional shielding.

Bundled fibres are held in ferrules which illuminate one end of the air-core light guides that penetrate through 42.5 cm of the shielding matrix (steel, lead, and polyethylene). This shielding is necessary to protect the photomultipliers and the front-end electronics housed in the read-out boxes. The air-core light guide consists of a hollow tube lined on the inside with highly reflective custom-made sheets. These metal-coated reflectors are designed to be very efficient ($> 90\%$) in the visible spectrum at the relevant angles (≈ 70 degrees from normal). Light typically makes five bounces before reaching the photocathode and nearly half the light is lost in this transport. Each light guide is coupled to a standard bialkaline, 8-stage photomultiplier tube with a borosilicate glass window. A read-out box (RBX) houses 24 PMTs and services half of a wedge (10° in ϕ).

The entire calorimeter system, with its shielding components, is mounted on a rigid table which supports more than 240 t with less than 1 mm deflection. The absorber alone weighs 108 t. The table is also designed for horizontal separation of the detector into two sections to clear the beam pipe at installation and removal. It is possible to align the forward calorimeters within ± 1 mm with respect to the rest of the CMS experiment.

2008 JINST 3 S08004

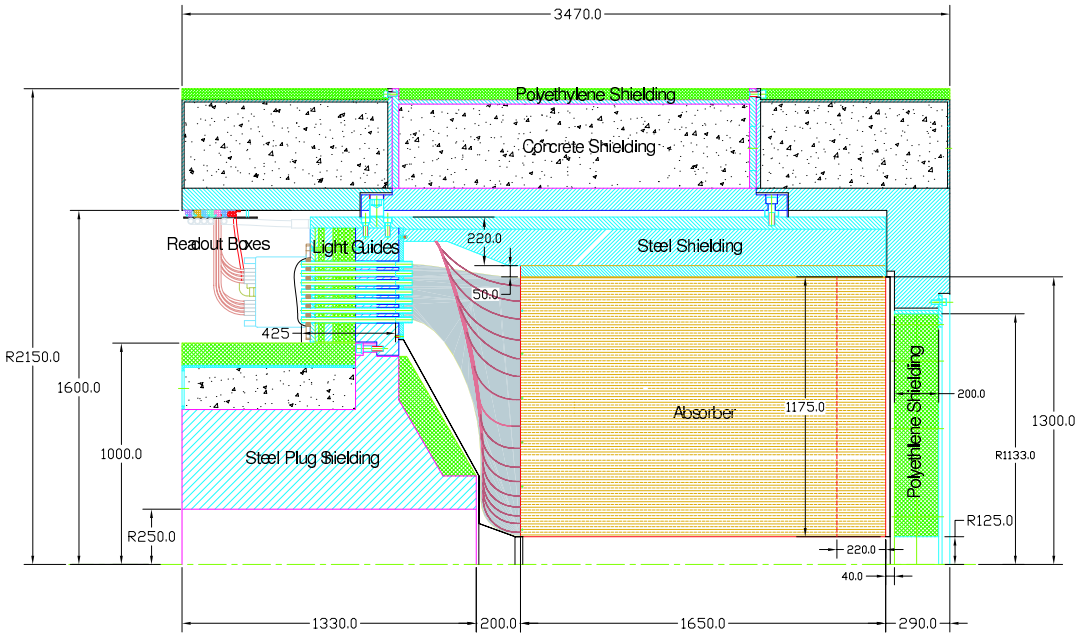

Figure 5.28: The cross sectional view of the HF calorimeter shows that the sensitive area extends from 125 to 1300 mm in the radial direction. The absorber in the beam direction measures 1650 mm. Bundled fibres (shaded area) are routed from the back of the calorimeter to air-core light guides which penetrate through a steel-lead-polyethlene shielding matrix. Light is detected by PMTs housed in the read-out boxes. Stainless steel radioactive source tubes (red lines) are installed for each tower and are accessible from outside the detector for source calibration. The interaction point is at 11.2 meters from the front of the calorimeter to the right. All dimensions are in mm.

The inner part of HF ($4.5 < |\eta| < 5$) will experience radiation doses close to 100 Mrad/year, and large neutron fluxes leading to activation of the absorber material, reaching several mSv/h in the region closest to the beam line after 60 days of running at $10^{34}\,\mathrm{cm}^{-2}\mathrm{s}^{-1}$ luminosity and one day of cooling down. The active elements of HF (quartz fibres) are sufficiently radiation-hard to survive these levels of radiation with limited deterioration. The PMTs are shielded behind 40 cm of steel and borated polyethylene slabs. HF, using Cherenkov light from quartz fibres, is practically insensitive to neutrons and to low energy particles from the decay of activated radionucleids. Further shielding around HF achieves activation levels below 10 μSv/h on the periphery of the detector. A 10-cm-thick lead plate, located in front of HF during operations around the detector, reduces personal exposure to radiation from the absorber. Maintenance of read-out boxes will be performed with the help of semi-automatic extractor tools. HF is equipped with radiation monitors located at the periphery of the detector, and with a system (Raddam) to measure the transmission properties of a few reference quartz fibres embedded in the absorber, as a function of integrated luminosity.

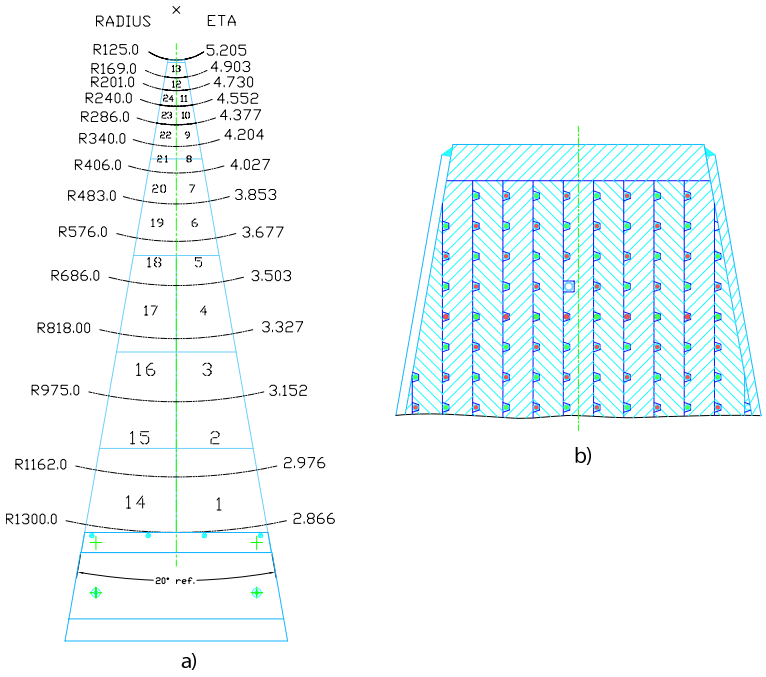

Figure 5.29: a) Transverse segmentation of the HF towers. b) An expanded view of the wedge shows the squared out groove holding the radioactive source tube.

Table 5.8: The tower sizes, number of fibres, bundle sizes and the percentage of photocathode area utilized are listed below for each tower. The air-core light guides are tapered to better match the photocathode area for towers 1, 2 and 3.

Ring No	$(r_{\text{in}}, r_{\text{out}})$ [mm]	$\Delta\eta$	$\Delta\phi$ [degree]	N_{fib}	A_{bundle} [mm^2]	$\frac{A_{\text{bundle}}}{A_{\text{photocathode}}}$
1	(1162–1300)	0.111	10	594	551	1.14
2	(975–1162)	0.175	10	696	652	1.33
3	(818–975)	0.175	10	491	469	0.96
4	(686–818)	0.175	10	346	324	0.66
5	(576–686)	0.175	10	242	231	0.47
6	(483–576)	0.175	10	171	167	0.34
7	(406–483)	0.175	10	120	120	0.25
8	(340–406)	0.175	10	85	88	0.18
9	(286–340)	0.175	10	59	63	0.13
10	(240–286)	0.175	10	41	46	0.94
11	(201–240)	0.175	10	30	35	0.71
12	(169–201)	0.175	20	42	52	0.11
13	(125–169)	0.300	20	45	50	0.10

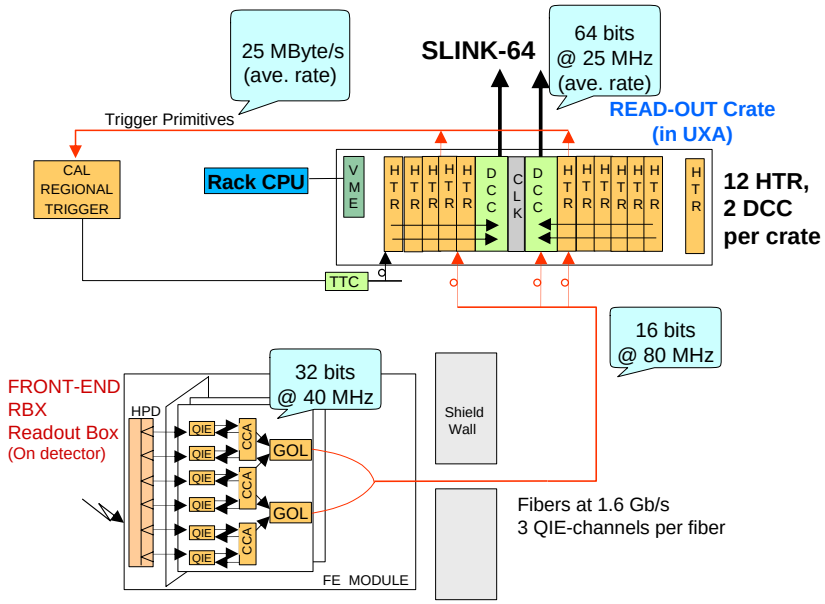

Figure 5.30: Overview of HCAL read-out electronics.

5.5 Read-out electronics and slow control

The overview of the full HCAL read-out chain is shown in figure 5.30. The read-out consists of an optical to electrical transducer followed by a fast charge-integrating ADC. The digital output of the ADC is transmitted for every bunch over a gigabit digital optical fibre to the service cavern, housing the off-detector electronics. In the service cavern, the signal is deserialized and used to construct trigger primitives which are sent to the calorimeter trigger. The data and trigger primitives are also pipelined for transmission to the DAQ upon a Level-1 Accept (L1A) decision.

The optical signals from the scintillator-based detectors (HB/HE/HO) are converted to electrical signals using multichannel hybrid photodiodes (HPDs) which provide a gain of ≈ 2000. A detailed view of the scintillator-based front-end read-out chain is given in figure 5.31. The optical signals from individual sampling layers are brought out on clear fibres. The fibres corresponding to a projective calorimeter tower are mapping via an optical decoding unit (ODU) to a cookie that interfaces to individual pixels on the HPD. In the forward calorimeter, where the magnetic fields are much smaller than in the central detector, conventional photomultiplier tubes (Hamamatsu R7525HA) are used and quartz-fibre bundles are routed directly to the phototube windows.

An overview of the HCAL controls is given in figure 5.32. Several PCs in the CMS control room operated through PVSS are used to control high and low voltages. The control system also downloads pedestal DAC and timing parameters to front-ends and controls many of the calibration and monitoring systems including the source calibration drivers, the LED pulsers, and the laser system. These systems record temperature, humidity and other constants useful for correlation studies of detector/calibration stability.

The configuration database contains the relationships or mapping for all HCAL detector components: wedges, layers, read-out boxes (RBX), cables, HCAL Trigger (HTR) cards, and calibra-

2008 JINST 3 S08004

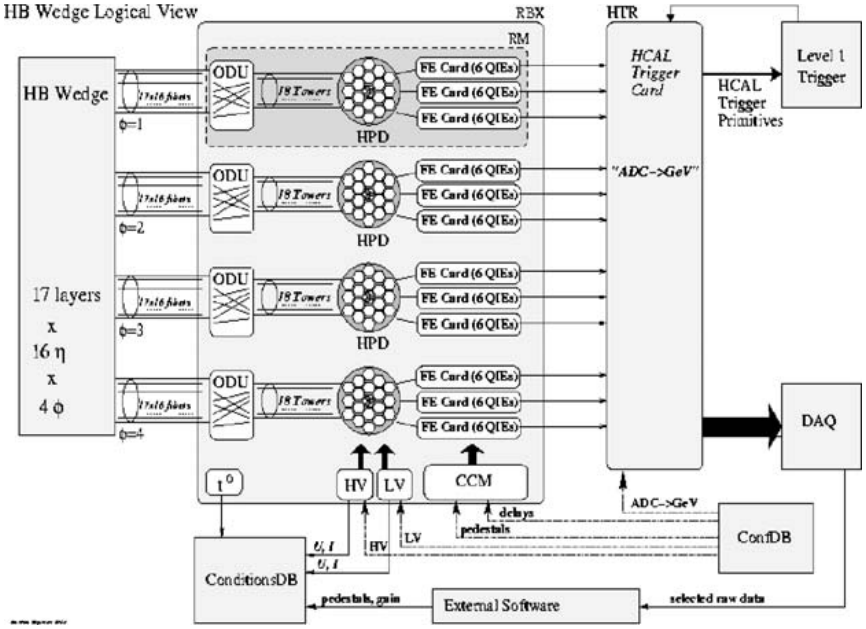

Figure 5.31: Overview of HCAL read-out/trigger chain and connections to database.

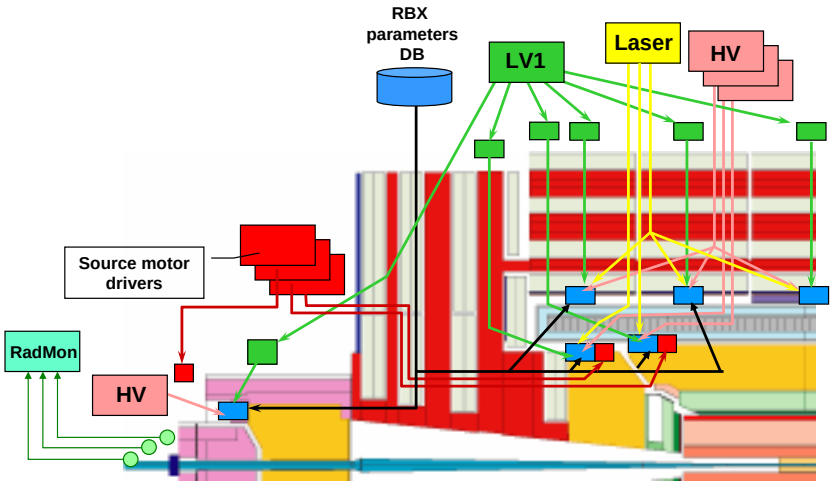

Figure 5.32: Overview of HCAL detector controls.

tion parameters for various components e.g. RBX, QIE, source types and strength. The conditions database has the slow-controls logging, the calibration constants (pedestals, gains, timing information, etc.) and the configuration database downloaded to the read-out system during the initialization.

The analogue signal from the HPD or photomultiplier is converted to a digital signal by a charge-integrating ADC ASIC called the QIE (Charge-Integrator and Encoder). The QIE internally contains four capacitors which are connected in turn to the input, one during each 25 ns period. The integrated charge from the capacitors is converted to a seven-bit non-linear scale to cover the

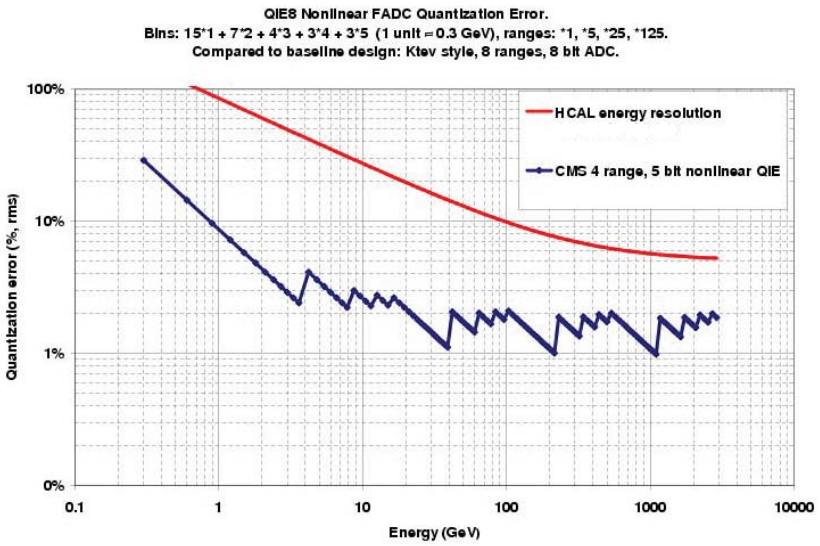

Figure 5.33: Contribution of the FADC quantization error to the resolution, compared with a representative HCAL resolution curve.

large dynamic range of the detector. The ADC is designed so its contribution to the detector energy resolution over its multi-range operation is negligible, as shown in figure 5.33. The QIE input characteristics were chosen from test beam data to optimize speed and noise performance. This resulted in a per channel RMS noise of 4600 electrons (0.7 fC) corresponding to about 180 MeV.

The digital outputs of three QIE channels are combined with some monitoring information to create a 32-bit data word. The 32-bit data, at a rate of 40 MHz, is fed into the Gigabit Optical Link (GOL) chip and transmitted using 8b/10b encoding off the detector to the service cavern. In the service cavern, the data is received by the HCAL Trigger/Read-out (HTR) board. The HTR board contains the Level-1 pipeline and also constructs the trigger primitives for HCAL. These trigger primitives are sent to the Regional Calorimeter trigger via Serial Link Board mezzanine cards. The HTR board receives data for 48 channels (16 data fibres) and may host up to six SLBs.

When a L1A is received by the HTR through the TTC system, it prepares a packet of data for the DAQ including a programmable number of precision read-out values and trigger primitives around the triggered bunch crossing. For normal operations, the HTR will transmit 7 time samples for each non-zero channel and a single trigger primitive for every trigger tower. These packets of data, each covering 24 channels, are transmitted by LVDS to the HCAL Data Concentrator Card (DCC). The DCC is the HCAL Front-End Driver (FED) and concentrates the data from up to 360 channels for transmission into the DAQ.

The Level-1 trigger primitives (TPG) are calculated in the HTR modules. The QIE data are linearized and converted to transverse energy with a single look up table. Two or more consecutive time samples are summed. A sum over depth is made for those towers having longitudinal segmentation. A final look up table is used to compress the data before sending the data across the trigger link to the regional calorimeter trigger. Table 5.9 summarizes the geometry of the trigger towers. The HF towers are summed in η and ϕ before being sent to the trigger.

2008 JINST 3 S08004

Table 5.9: Sizes of the HCAL trigger towers in η and ϕ.

Tower index	$\lvert\eta_{\max}\rvert$	Detector	Size	
			η	ϕ
1–15	$0.087\times\eta$	HB	0.087	5°
16	1.392	HB, HE	0.087	5°
17–20	$0.087\times\eta$	HE	0.087	5°
21	1.830	HE	0.090	5°
22	1.930	HE	0.100	5°
23	2.043	HE	0.113	5°
24	2.172	HE	0.129	5°
25	2.322	HE	0.150	5°
26	2.500	HE	0.178	5°
27	2.650	HE	0.150	5°
28	3.000	HE	0.350	5°
29	3.314	HF	0.461	20°
30	3.839	HF	0.525	20°
31	4.363	HF	0.524	20°
32	5.191	HF	0.828	20°

Timing and synchronization

The QIE integration clock is controlled by the Channel Control ASIC (CCA) which allows for fine-skewing of the integration phase of each tower relative to the machine clock. This allows each channel's integration phase to correct for differences in the time-of-flight from the interaction region as well as differences in the optical pathlength within the detector.

Figure 5.34 shows that scintillator tile signals produce relatively fast pulses such that 68% of the pulse is contained within a 25 ns window. Figure 5.35 shows the pulse shape for the forward calorimeter. The Cerenkov process and the phototubes used in the forward calorimeter are extremely fast, so the pulse in HF is only 10 ns wide. The HF is thus subject only to in-time pile-up which is important in the highly active forward region of CMS.

An additional important effect on the HCAL pulse timing in HB/HE/HO comes from the input stage of the QIE. The QIE has an amplitude-dependent impedance which implies a faster pulse shape for large signals than for small ones, as seen in figure 5.36. The amount of time slewing is dependent on the noise characteristics of the QIE, so the final QIE ASICs for the barrel and endcap were chosen to limit the timeslew to the "medium" case in exchange for somewhat increased noise. In the outer calorimeter, the noise level is a critical factor for muon identification and pile-up is much less important so the quieter "slow" characteristics were chosen for the HO QIEs.

The in-situ synchronization of HCAL is performed using the HCAL laser system. The laser system consists of a single UV laser which can illuminate an entire half-barrel of HB or a single endcap at once through a series of optical splitters. The quartz fibres which lead from the laser to the detector have been carefully controlled to equalize the optical path length to each wedge. The laser can be directed either straight onto a scintillator block connected to the HPD or into the

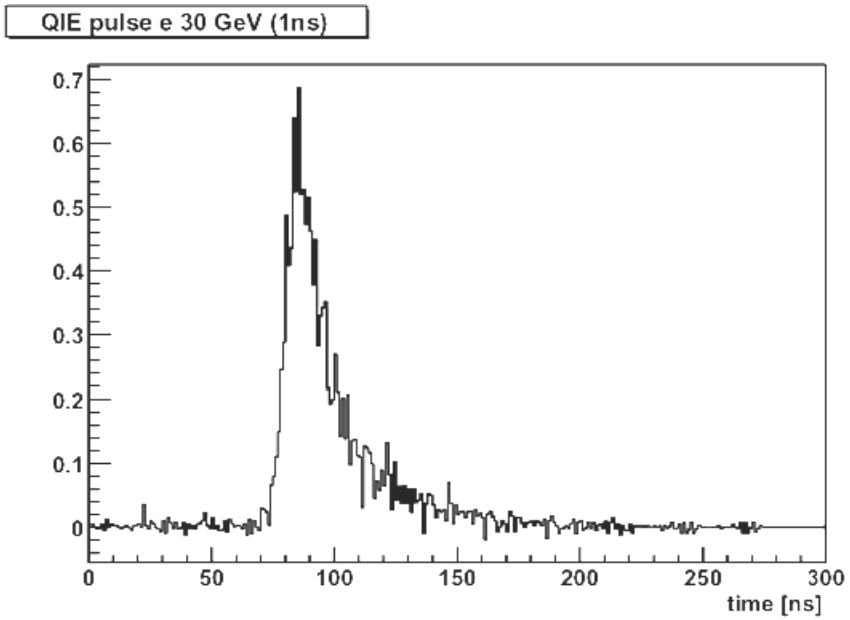

Figure 5.34: Measured single event pulse shape from the scintillator tiles, representative of HB/HE/HO pulse shapes.

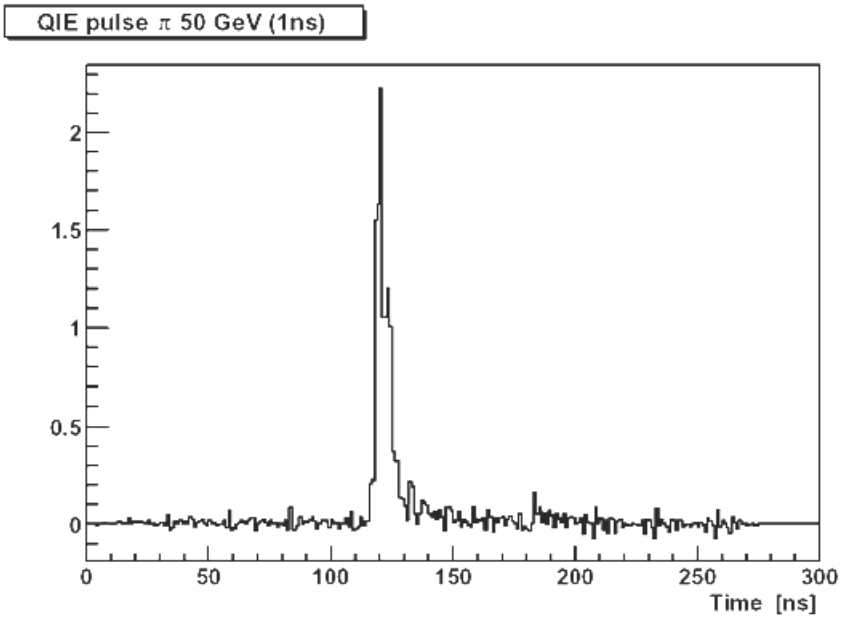

Figure 5.35: Measured pulse shape, energy collected vs. time, for HF.

wedge. Within layer 9 of each wedge is an arrangement of optical fibres which mimic the time-of-flight from the interaction region. This arrangement allows the timing of HCAL to be flattened and monitored, as has been demonstrated in test beam data taking, which verified the timing determined by the laser using the synchronized beam. In the HO and HF detectors, only the photodetector can be illuminated so the alignment will be based on construction and test beam data.

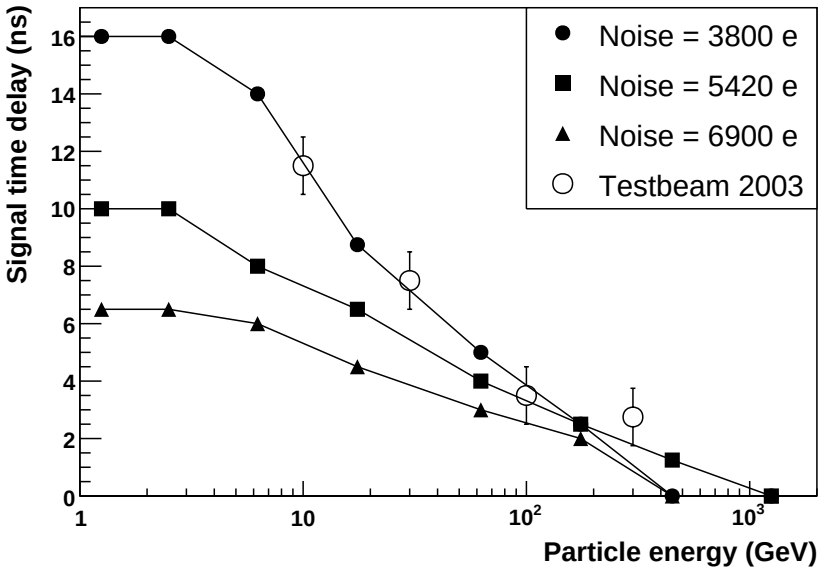

Figure 5.36: Pulse time variation as a function of signal amplitude as measured on the bench (solid points) for several input amplifier configurations compared with test beam measurements from 2003.

The channel-by-channel bunch synchronization of HCAL will be determined using a histogramming procedure in the serial link boards (SLBs) which determine the bunch synchronization using the beam structure of the LHC. The event and bunch synchronization is monitored using fast control signals originating from the TTC system which are transmitted in the data stream between the front-ends and the HTR. On a global scale, the bunch and event synchronization between the HCAL and other detector subsystems is determined using muons and other correlated physics signals.

5.6 HF luminosity monitor

The CMS luminosity measurement will be used to monitor the LHC's performance on a bunch-by-bunch basis in real time and to provide an overall normalization for physics analyses. The design goal for the real-time measurement is to determine the average luminosity with a 1% statistical accuracy with an update rate of 1 Hz. For offline analyses, the design goal is a systematic accuracy of 5%, although every reasonable effort will be made to produce a more accurate result. Both of these requirements must be met over a very large range of luminosities, extending from roughly 10^{28} cm^{-2}s^{-1} to 10^{34} cm^{-2}s^{-1}, and possibly beyond.

A number of techniques capable of providing suitable luminosity information in real time have been identified [17]. One technique employs signals from the forward hadron calorimeter (HF) while another, called the Pixel Luminosity Telescope (PLT), uses a set of purpose-built particle tracking telescopes based on single-crystal diamond pixel detectors. At the time of writing, the PLT has not been formally approved, but is under study. The methods based on signals from the HF are the ones being most vigorously pursued.

Two methods for extracting a real-time relative instantaneous luminosity with the HF have been studied. The first method is based on *zero counting* in which the average fraction of empty towers is used to infer the mean number of interactions per bunch crossing. The second method exploits the linear relationship between the average transverse energy per tower and the luminosity.

Outputs of the QIE chips used to digitize the signals from the HF PMTs on a bunch-by-bunch basis are routed to a set of 36 HCAL Trigger and Read-out (HTR) boards, each of which services 24 HF physical towers. In order to derive a luminosity signal from the HTR, an additional mezzanine board called the HF luminosity transmitter (HLX) is mounted on each of the HTR boards. The HLX taps into the raw HF data stream and collects channel occupancy and E_T-sum data and transmits them to a central collector node over standard 100-Mbps Ethernet. The HLX boards have the same form factor as the Synchronization and Link Boards (SLBs) used to interface the ECAL and HCAL readouts to the Regional Calorimeter Trigger (RCT) system.

Although all HF channels can be read by the HLX, MC studies indicate that the best linearity for occupancy histograms is obtained using just two η rings. Hence two sets of two rings are used for the occupancy histograms. Four rings are combined to form the E_T-sum histogram. The algorithm has been optimized to minimize sensitivity to pedestal drifts, gain changes and other related effects. Each of the two sets of rings sends 12 bits of data to the HLX. There are three occupancy histograms dedicated to each of the following possible states for each tower: enabled-below-threshold, over-threshold-1, over-threshold-2. In addition, a 15-bit E_T sum value is sent to the HLX and a further histogram based on all 13 HF η rings is filled for use by the LHC. As a result, the input to the HLX is used to create eight histograms: two sets of three occupancy histograms, one E_T-sum histogram, and one additional occupancy histogram.

Each histogram has 3564 bins, one for each bunch in the LHC orbit. Each occupancy-histogram bin uses two bytes, and there are four bytes per bin in the E_T sum histogram. The baseline design is to add the results from all desirable channels into a single set of histograms.

The histograms are transmitted as UDP (User Datagram Protocol) packets from the HLX cards once roughly every 0.37 s, which is safely within the 1.45 s (worst case) histogram overflow time. The Ethernet core in the HLX automatically packages the data to make optimal use of network bandwidth. Each histogram spans several Ethernet packets, the precise number depending on the type of histogram. The eight sets of histograms comprise about 70 kB of data, which is transmitted at a rate of approximately 1.6 Mbps to an Ethernet switch that aggregates the data from multiple HLX boards. The switch multi-casts the data to a pair of luminosity server nodes. One of the servers is responsible for publishing the luminosity information to various clients, such as the CMS and LHC control rooms and the Fermilab Remote Operations Center (ROC). The second server archives the data for each luminosity section (one luminosity section corresponds to 2^{20} orbits, or about 93 s). An XDAQ layer on this server makes it possible to communicate with other CMS DAQ systems.

2008 JINST 3 S08004